**CNWRA** *A center of excellence in earth sciences and engineering*

A Division of Southwest Research Institute™
6220 Culebra Road • San Antonio, Texas, U.S.A. 78228-5166
(210) 522-5160 • Fax (210) 522-5155

September 21, 2000
Contract No. NRC–02–97–009
Account No. 20.01402.671

U.S. Nuclear Regulatory Commission
ATTN: Dr. Mysore S. Nataraja
Division of Waste Management
TWFN Mail Stop 7–C6
Washington, DC 20555

Subject: Repository Design and Thermal-Mechanical Effects Key Technical Issue Intermediate Milestone 20.01402.671.020, DECOVALEX Thermal-Mechanical-Hydrologic Coupled Analysis—Progress Report

Dear Dr. Nataraja::

The attached is the Center for Nuclear Waste Regulatory Analyses document entitled: Progress Report for DECOVALEX III Task 2: Numerical Simulation of the Drift-Scale Heater Test at Yucca Mountain. To better reflect the content of the document, the title has been changed from that originally identified in the Operations Plan. This technical document fulfills the requirements for the subject milestone which is due September 22, 2000.

This report summarizes recent analyses of the U.S. Department of Energy Drift-Scale Heater Test (DST). This report was prepared as part of the DECOVALEX project to independently evaluate MULTIFLO, a thermal-hydrological (TH) model used by NRC in calculations to support their high-level waste regulatory program, and compare MULTIFLO results with results from other TH codes. The DST at Yucca Mountain (YM) has been used to provide a basis to assess the capability of the TH codes to simulate complex TH processes. This modeling study is an important part of assessing and developing confidence in the predictive models used to evaluate the safety case for the geologic repository at YM.

The analyses reported in this document include refinements made in the DST numerical model to reduce differences between predicted and simulated temperatures. Refinements that reduced the differences were a factor of 1,000 reduction in fracture permeability and a 20-percent reduction in thermal conductivity to all three geologic units simulated in the model. In addition, the effect of mass loss through the thermal bulkhead was investigated. It was found that a mass removal of 80 mL/hr of liquid from the drift wall resulted in indistinguishable differences in predicted temperature, but small observable differences in predicted fracture saturation.

Washington Office • Twinbrook Metro Plaza #210
12300 Twinbrook Parkway • Rockville, Maryland 20852-1606

If you have any questions on this report, please contact me at (210) 522-5151 or Dr. Ronald Green at (210) 522-5305.

Sincerely yours,

Asadul H. Chowdhury, Manager
Mining, Geotechnical, and
Facility Engineering

AHC/ph
Enclosure

cc:
J. Linehan (w/o enclosure)
D. DeMarco
B. Meehan
E. Whitt
J. Holonich
W. Reamer
B. Jagannath
D. Galvin
K. Stablein
T. Essig
D. Brooks
T. McCartin
P. Justus
J. Greeves
R. Codell
B. Leslie
J. Trapp
W. Patrick
CNWRA Directors
CNWRA Element Mgrs
T. Nagy (SwRI Contracts)
P. Maldonado
R. Green
S. Painter
S. Hsiung
A. Ghosh
B. Dasgupta
M. Hill

# PROGRESS REPORT FOR DECOVALEX III TASK 2: NUMERICAL SIMULATION OF THE DRIFT-SCALE HEATER TEST AT YUCCA MOUNTAIN

*Prepared for*

**Nuclear Regulatory Commission**
**Contract NRC–02–97–009**

*Prepared by*

**Ronald T. Green**
**Scott L. Painter**
**Melissa E. Hill**

**Center for Nuclear Waste Regulatory Analyses**
**San Antonio, Texas**

**September 2000**

# ABSTRACT

This report documents recent analyses conducted as part of the DECOVALEX III task 2 initiative. The Drift-Scale Heater Test (DST) at the Exploratory Studies Facility at Yucca Mountain was designated for study under task 2 of the DECOVALEX III program. This report will be the basis for a formal report documenting Center for Nuclear Waste Regulatory Analyses (CNWRA) thermal-hydrological (TH) modeling analysis of the DST to predict the temperature and saturation distribution in the rock during the heating and cooling phases of the test. The outcome of this predictive analysis is compared with measured temperatures and saturations to guide refinement of the model. TH modeling results will be used subsequently to perform thermal-hydrological-mechanical analyses. These modeling studies are an important part of the process of assessing and developing confidence in both U.S. Department of Energy models and those developed on behalf of the U.S. Nuclear Regulatory Commission to independently evaluate the safety case for the proposed geologic repository at Yucca Mountain.

The basis for the conceptual and numerical models used in these analyses is presented in this report. Modeling results of the DST reported here build on previous CNWRA results (Green et al., 2000). Analyses conducted as part of this study evaluated the importance of values assigned to fracture permeability and thermal conductivity in model predictions. Model predictions were evaluated by comparing simulated temperatures and temperatures measured in two boreholes at the DST after one year of heating. It was found that a factor of 1,000 reduction in fracture permeability and a 20-percent reduction in thermal conductivity resulted in the greatest reduction in temperature difference. In addition, the effect of mass loss through the thermal bulkhead was investigated. It was found that mass removal of 80 mL/hr of liquid from the drift wall resulted in indistinguishable differences in predicted temperature, yet small observable differences in predicted fracture saturation. Additional refinements to the conceptual and numerical models to investigate heat and mass transport at the DST are proposed based on the results of this study.

# CONTENTS

# FIGURES

# FIGURES (cont'd)

# TABLES

# ACKNOWLEDGMENTS

This report documents work performed by the Center for Nuclear Waste Regulatory Analyses (CNWRA) for the U.S. Nuclear Regulatory Commission (NRC) under Contract No. NRC–02–97–009. The activities reported here were performed on behalf of the NRC Office of Nuclear Material Safety and Safeguards, Division of Waste Management. The report is an independent product of the CNWRA and does not necessarily reflect the views or regulatory position of the NRC.

The authors thank G. Ofoegbu and W. Patrick for technical and programmatic reviews of this document. The authors are thankful to P. Houston for skillful typing of the report and to B. Long for providing a full range of editorial services in preparation of the final document. The authors also thank D. Coffin for assistance with performing MULTIFLO simulations and M. Seth for assistance in assessing applications of the MULTIFLO code.

# QUALITY OF DATA, ANALYSES, AND COMPUTER CODES

**DATA:** No CNWRA-generated original data are contained in this report.

**ANALYSES AND CODES:** MULTIFLO Version 1.2 software developed under CNWRA quality assurance procedures was used in all analyses reported in this document.

# 1 INTRODUCTION

## 1.1 BACKGROUND

DECOVALEX (acronym for the **DE**velopment of **CO**upled models and their **VAL**idation against **EX**periments in nuclear waste isolation) is an international cooperative project to support the development of mathematical models of coupled processes in the geosphere and in their applications and validation against experiments in the field of nuclear waste isolation. The DECOVALEX project has been organized to increase understanding of thermal-hydrological-mechanical (THM) processes for rock mass stability and radionuclide release and transport from a repository to the biosphere and also assess how these processes can be described by mathematical models. DECOVALEX contains three phases. DECOVALEX I began in 1991 and was completed in 1995. In this phase, the activities focused on modeling benchmark problems and laboratory experiments. The U.S. Nuclear Regulatory Commission (NRC) was one of the founding members of DECOVALEX I and an active participant. The Center for Nuclear Waste Regulatory Analyses (CNWRA) assisted NRC in performing analysis work. DECOVALEX II started in 1995 and ended in 1999. The focus of this phase was using the modeling experience gained during the first phase to simulate experiments conducted in the field. The NRC and CNWRA did not participate in this phase of the project. DECOVALEX III began in 1999. This third phase of the project includes four tasks. Task 1 involves modeling FEBEX (**F**ull-scale **E**ngineered **B**arriers **EX**periment) *in situ* experiments. Task 2 involves modeling and predicting the drift-scale heater test (DST) at Yucca Mountain (YM). Task 3 includes three benchmark problems. The first benchmark deals with the implications of THM coupling on the near-field performance of a nuclear waste repository. The second benchmark investigates the effects of upscaling THM processes on performance assessment results. The third benchmark studies the effect of glaciation on rock mass behavior. Task 4 attempts to address the issue of applying the effects of THM processes to performance assessment. The NRC, with the assistance of the CNWRA, is actively participating in the DECOVALEX III project. Task 2 is the focus of NRC involvement. This report presents the results of analysis for the DST at YM, because this work is most relevant to the high-level waste program.

## 1.2 OBJECTIVE AND SCOPE

This report documents analyses conducted by the CNWRA as part of the DECOVALEX III task 2 project. The DST at the Exploratory Studies Facility (ESF) at YM was designated for study under task 2 of DECOVALEX III. Two exercises have been identified within task 2:

- Part A. Perform a thermal-hydrologic (TH) modeling analyses of the DST to predict the temperature and saturation distribution in the rock during the heating and cooling phases of the test. The outcome of this predictive analysis is the basis for comparing with measured temperatures and saturations to guide refining the model.

- Part B. Given the temperature distribution, perform a THM analysis of the test to predict the displacements in the rock at various times during the heating and cooling phases of the test. Comparative analyses of the predicted and measured displacements are to be used to enable refining the THM model.

Only part A of task 2 is active at this time. Results from the TH modeling analyses are reported in this document. The topics addressed in this report are (i) justification and definition of the mathematical model used in the TH analyses, (ii) justification of the values adopted for the parameters defining the

mathematical model, and (iii) numerical solution of the mathematical model. These modeling studies are an important part of the process of assessing and developing confidence in both U.S. Department of Energy models and those developed on behalf of the U.S. Nuclear Regulatory Commission to independently evaluate the safety case for the proposed geologic repository at YM.

# 2 MATHEMATICAL SETTING

The MULTIFLO code, Version 1.2, was used in all analyses reported in this document (Lichtner et al., 2000). MULTIFLO is a general code for simulating multiphase, multicomponent, transport processes in nonisothermal systems with chemical reactions and reversible and irreversible phase changes in solids, liquids, and gases. The following description of MULTIFLO is taken from Lichtner et al. (2000).

The MULTIFLO code consists of two sequentially coupled submodules: Mass and Energy TRAnsport (METRA) and General Electrochemical Migration (GEM). GEM solves mass balance equations for multicomponent reactive transport of solute species. METRA solves mass balance equations for water and air and an energy balance equation. GEM solves mass balance equations for multicomponent reactive transport of solute species. Only transport of air, water, and heat was simulated in these analyses; therefore only the METRA submodule was used in these analyses. Chemical transport at the DST is not investigated as part of this analysis.

METRA represents multiphase flow through three dimensions, although zero, one, or two dimensions are also possible. Single phase (i.e., all liquid or all gas) or two-phase systems can be simulated. The equation of state for water in METRA allows temperatures in the range 1–800 °C and pressures below 165 bars. A description of mathematical basis for METRA is presented in this section. A discussion of the balance equations is followed by the constitutive equations and the dual continuum model formulation. The conservation equation for the water component ($w$) is given by

$$\frac{\partial}{\partial t}\left[\varphi\left(s_l n_l X_w^l + s_g n_g X_w^g\right)\right] + \nabla\cdot\left(q_l n_l X_w^l + q_g n_g X_w^g - D_g^{\text{eff}} n_g \nabla X_w^g\right) = Q_w \qquad (2\text{-}1)$$

and for the air component ($a$) by

$$\frac{\partial}{\partial t}\left[\varphi\left(s_l n_l X_a^l + s_g n_g X_a^g\right)\right] + \nabla\cdot\left(q_l n_l X_a^l + q_g n_g X_a^g - D_g^{\text{eff}} n_g \nabla X_a^g\right) = Q_a \qquad (2\text{-}2)$$

with source terms $Q_w$ and $Q_a$ and where $\varphi$ is porosity. In these equations, mass transport, $q_l$ and $q_g$, is represented by Darcy's Law (as modified by the relative permeability for multiphase flow), which includes capillarity, gravity, and viscous forces

$$q_l = -\frac{k k_l}{\mu_l}\nabla\left(P_l - \rho_l g z\right) \qquad (2\text{-}3)$$

and

$$q_g = -\frac{kk_g}{\mu_g}\nabla\left(P_g - \rho_g gz\right) \tag{2-4}$$

where $k$ denotes the saturated permeability, $P_{l,g}$ the fluid pressure, $\mu_{l,g}$ the viscosity with mass densities $\rho_{l,g}$, $g$ the acceleration of gravity, and where subscripts $l$ and $g$ denote the liquid and gas (vapor) phases. The terms $n_{l,g}$ refer to the density of the liquid and gas phases based on a molar representation. Gas mixture properties are calculated assuming the ideal gas law. Gas viscosity is calculated using the kinetic theory of gases (Hirschfelder et al., 1954). The mole fractions $X_w^{l,g}$ and $X_a^{l,g}$ satisfy the relations

$$X_w^l + X_a^l = 1 \tag{2-5}$$

and

$$X_w^g + X_a^g = 1 \tag{2-6}$$

Diffusion of water in the aqueous phase is neglected. The liquid and gas pressures are related through the capillary pressure

$$P_l = P_g - P_c \tag{2-7}$$

The effective binary gas diffusion coefficient is defined using temperature, pressure, and material properties by

$$D_g^{\text{eff}} = \omega\,\tau\,\varphi\,s_g D_g^o \frac{P_o}{P}\left[\frac{T+T_o}{T_o}\right]^\theta \tag{2-8}$$

where $T_o$ and $P_o$ denote reference temperature and pressure, $\tau$ is tortuosity, $\theta$ is an empirical constant, and $\omega$ is an enhancement factor (Walton and Lichtner, 1995). The enhancement factor is usually considered to be inversely proportional to the gas saturation, $s_g$, which cancels from the expression for the effective gas diffusion coefficient.

Adding Eqs. (2-1) and (2-2) eliminates the diffusive terms providing the total mass balance equation for air and water as

$$\frac{\partial}{\partial t}\left[\varphi\left(s_l n_l + s_g n_g\right)\right] + \nabla\cdot\left(q_l n_l + q_g n_g\right) = Q_w + Q_a \tag{2-9}$$

Energy transfer is by convection and conduction. The energy balance equation, assuming thermodynamic equilibrium between rock and fluid, is given by

$$\frac{\partial}{\partial t}\left[\varphi\left(s_l n_l U_l + s_g n_g U_g\right)\right] + \nabla\cdot\left(q_l n_l H_l + q_g n_g H_g\right)$$
$$+\frac{\partial}{\partial t}\left[(1-\varphi)C_P^{\text{rock}}\rho_{\text{rock}}T\right] - \nabla\cdot\kappa\nabla T = Q_e \tag{2-10}$$

where $U_{l,g}$ denotes the total internal energy, $H_{l,g}$ the total enthalpy of the designated fluid phase, $C_P^{\text{rock}}$ the heat capacity, $\kappa$ the thermal conductivity, and $Q_e$ a source term. Heat produced by chemical reaction is not included in the present version of the code. Energy transfer by radiation is only included at a boundary. Mass transfer in the gas phase may be enhanced by binary gas diffusion.

Vapor-pressure lowering of water-phase behavior resulting from capillary forces is defined by Kelvin's equation

$$P_v = P_{\text{sat}}(T)e^{-Pc/n_l RT} \tag{2-11}$$

where $P_v$ represents vapor pressure, $P_{\text{sat}}$ the saturation pressure of pure water, $T$ the absolute temperature, and $R$ the gas constant. Note that the density of the liquid phase, $n_l$, is represented on a molar basis.

Spatially variable values for porosity, absolute rock permeability (variable in three spatial directions), tortuosity, thermal conductivity, and media characteristic curves for relative permeability and capillary pressure can be specified. Capillary saturation relations provided in METRA are van Genuchten (1980), linear, and Brooks-Corey (Brooks and Corey, 1966) functions.

Relative liquid permeability, $k_{rl}$, for flow between the continua is calculated as the upstream weighted average of the fracture and matrix permeabilities. Relative liquid permeability for the fracture and matrix continua is calculated using the Mualem relationship (Mualem, 1976)

$$k_{rl} = \sqrt{s_l^{\text{eff}}}\left\{1-\left[1-\left(s_l^{\text{eff}}\right)^{1/\lambda}\right]^{\lambda}\right\}^2 \tag{2-12}$$

where capillary pressure is related to saturation by the van Genuchten relationship (van Genuchten, 1980)

$$s_l^{\text{eff}} = \left[1+\left(\alpha|P_c|\right)^m\right]^{-\lambda} \tag{2-13}$$

effective liquid saturation, $s_l^{\text{eff}}$, is defined

$$s_l^{\text{eff}} = \frac{s_l - s_l^{res}}{s_l^o - s_l^r} \tag{2-14}$$

and where *res* and *o* denote residual and maximum saturations. $\lambda$ is related to m in Eq. (2-13) by $\lambda = 1 - 1/m$.

The gas phase relative permeability is defined

$$k_{rg} = 1 - k_{rl} \tag{2-15}$$

The Brooks-Corey functions for relative permeability are defined by (Brooks and Corey, 1966)

$$k_{rl} = s_*^4 \tag{2-16}$$

and

$$k_{rg} = \left(1 - s_*^2\right)\left(1 - s_*\right)^2 \tag{2-17}$$

where

$$s_* = \frac{s_l - s_l^r}{1 - s_l^r - s_g^r} \tag{2-18}$$

The linear relations for relative permeability are defined

$$k_{rl} = s_* \tag{2-19}$$

and

$$k_{rg} = 1 - k_{rl} \tag{2-20}$$

where

$$s_* = \frac{s_l - s_l^r}{1 - s_l^r} \tag{2-21}$$

Thermal conductivity is also defined as a function of saturation (Somerton et al., 1974)

$$\kappa = \kappa(sat) + \sqrt{s_l^{\text{eff}}}\left\{\kappa(sat) - \kappa(dry)\right\} \tag{2-22}$$

where $\kappa(sat)$ and $\kappa(dry)$ are the thermal conductivities under fully saturated and dry conditions.

The dual continuum model (DCM) formulation is similar to the dual permeability model (DKM) formulation used in recent U.S. Department of Energy numerical simulations (TRW Environmental Safety Systems, Inc., 2000). The DCM and DKM conceptualizations provide separate continua for the matrix and the fractures. The dual continua are coupled throughout the model domain by transfer functions for heat and mass transfer

between the fractures and matrix. Use of a DCM increases the complexity of the numerical model used in the simulations, but offers the potential to realistically partition flow between matrix and fractures. The following is a description of key components to the DCM incorporated in MULTIFLO and used in the numerical analyses of the DST.

One of the critical parameters in a DCM-based simulation is the block size. Block size directly affects two model properties: (i) the interfacial area between the matrix and fracture continua in a DCM and (ii) the gradients that drive heat and mass between the two continua. In particular, increasing block size reduces the area available for heat and mass transfer between the matrix and fracture continua and increases the distance over which changes in pressure and temperature occur, thereby reducing their respective gradients.

The interfacial area between the two continua, $A_{fm}$, is defined using block dimensions, $l_i$, where $i = x, y,$ and z. For two dimensions the interfacial area is defined

$$A_{fm} = 2\left(1-\varepsilon_f\right)\left[\frac{1}{l_x}+\frac{1}{l_z}\right] \tag{2-23}$$

which for a cubic block geometry in two dimensions (i.e., $l_x = l_z$) becomes

$$A_{fm} = 4\left(\frac{1-\varepsilon_f}{l}\right) \tag{2-24}$$

where $\varepsilon_f$ is fracture porosity.

Mass flow across the matrix/fracture interface is directionally dependent. Liquid flow from the matrix to the fracture continuum is defined

$$Q_{l-\text{mass}} = \frac{A_{fm}A_{\text{mod}}}{\mu_l}k_{\text{harmonic}}k_r\frac{P_{lf}-P_{lm}}{d} \tag{2-25}$$

for $P_{lf} > P_{lm}$ liquid flow from the fracture to the matrix is defined

$$Q_{l-\text{mass}} = \frac{A_{fm}A_{\text{mod}}A^*_{\text{mod}}}{\mu_l}k_{\text{harmonic}}k_r\frac{P_{lf}-P_{lm}}{d} \tag{2-26}$$

for $P_{lf} > P_{lm}$ where the $m, f, l,$ and $r$ subscripts denote matrix, fracture, liquid, and relative. The term $d$ is the distance between the center of the matrix block and the center of the fracture defining the edge of the block. The fracture-matrix distance is related, but not equivalent, to block size. For the case where the element is a cube, $d = l/2 + \delta/2$, and where $\delta$ is the fracture aperture. Fracture aperture is calculated using block size, element size, and fracture porosity.

$A_{mod}$ is a modifier term included to allow a reduction, but not an increase, in the interfacial area between the matrix and fracture continua. An additional area modifier term, $A^*_{mod}$, is included in Eq. (2-26) to permit additional reduction in the interfacial area experienced with flow from the fracture to the matrix continuum when fractures are less than fully saturated. For a tuff with low matrix permeability and partially saturated fractures, a value of 1.0 is typically assigned to $A_{mod}$, and a significantly smaller value (e.g., $5.0 \times 10^{-4}$) is assigned to $A^*_{mod}$. A value of 1.0 assigned to $A_{mod}$ does not restrict flow for the matrix to the fracture. The unrestricted flow of gas from the matrix to the fracture ensures unrealistic pressures in the matrix are avoided. Assigning small values to $A^*_{mod}$ restricts the flow of water from the fractures to the matrix, thereby allowing fracture flow when the matrix is less than fully saturated.

The harmonic mean for liquid permeability is expressed as

$$k_{\text{harmonic}} = \frac{k_f\, k_m}{k_f + k_m} \tag{2-27}$$

An analogous form of Eq. (2-25) defines mass flow of gas between the matrix and fracture continua.

$$Q_{g-\text{mass}} = \frac{A_{fm} A_{\text{mod}}}{\mu_g} k_{\text{harmonic}} k_r \frac{P_{gf} - P_{gm}}{d} \tag{2-28}$$

Note that mass flow of gas between the matrix and fracture continua is not directional, that is, the $A_{mod}$ for matrix to fracture gas flow is equal to the $A_{mod}$ for fracture to matrix gas flow. The relative gas permeability is specified as the complement to relative liquid permeability

$$k_{rg} = 1 - k_{rl} \tag{2-29}$$

Analogous to mass flow are expressions and relationships for heat flow. Heat flow across the matrix fracture interface is defined

$$Q_{\text{heat}} = A_{fm} A_{\text{mod}}\, \kappa_{\text{arithmetic}} \frac{T_f - T_m}{d} \tag{2-30}$$

Note that heat transfer and mass transfer across the matrix/fracture interface are coupled processes, but each responds to its respective driving forces calculated for the same distance, *d*. Gradients that drive mass and heat transfer are decreased when the block dimensions are increased (i.e., the differences in pressure or temperature between the two continua remain the same for each model element while the distance over which the difference occurs increases with an increased block size, thereby reducing the gradients).

Either time-dependent Neumann (constant flux), Dirichlet (constant field variables), or mixed boundary conditions may be specified in MULTIFLO. Time-varying heat and mass sources and sinks may be designated at specified nodal locations. Time-varying boundary conditions, sources, or sinks are specified in tabular form and are linearly interpolated corresponding to the midpoint of the time step.

# 3 NUMERICAL SOLUTION

METRA is based on a fully implicit formulation using a variable substitution approach. Space discretization is based on a block-centered grid using an integral finite-volume difference scheme. This approach is suitable for structured and unstructured grid with arbitrary interblock grid connectivity and any polygon block boundary. Flow through fractured media may be represented by the DCM or as an equivalent continuum medium (ECM) where the dual continuum is represented by an equivalent single continuum (Pruess and Narasimhan, 1985; Klavetter and Peters, 1986).

Three primary variables are required to describe a two-phase nonisothermal system consisting of two species, water and air. The chosen primary variables are listed in table 3-1, where $P_l$ is the liquid pressure for a pure liquid system and $P_g$ the total gas pressure for a two-phase or pure gas-phase system. $X_a$ denotes the mole fraction of air with partial pressure $P_a$, $s_g$ denotes gas saturation, and $T$ denotes temperature.

Three primary equations are solved by METRA: (i) total mass balance, (ii) air mass balance, and (iii) energy balance. The three equations are simultaneously solved for each grid block by the tridiagonal Thomas algorithm for one-dimensional systems and, optionally, by the WATSOLV package (van der Kwaak et al., 1995). The WATSOLV package is based on incomplete factorization accelerated by employing generalized minimum residual or biconjugate gradient stabilized procedures suitable for both two-dimensional (2D) and three-dimensional systems (van der Kwaak et al., 1995).

**Table 3-1. Choice of primary variable for different fluid states**

| Fluid state | Primary variables |
|---|---|
| Single-phase liquid | $P_l$, $X_a$, $T$ |
| Two phase | $P_g$, $P_a$, $s_g$ |
| Single-phase gas | $P_g$, $P_a$, $T$ |

# 4 DRIFT-SCALE HEATER TEST MODEL

The ESF Thermal Test Facility (Alcove 5) is located in the Topopah Spring middle nonlithophysal (Tptpmn) unit, within the horizon of the proposed YM repository (TRW Environmental Safety Systems, Inc., 1997a). The Tptpmn unit is approximately 30–40 m thick at the location of the DST, overlain by the Topopah Spring upper lithophysal (Tptpul) and underlain by the Topopah Spring lower lithophysal (Tptpll) units. Alcove 5 is at Construction Station 28 + 27 [a coordinate system in meters (m) following the axis of the ESF and originating at the North Portal], just past the bend from the North Ramp to the Main Drift (as shown in figure 4-1 taken from TRW Environmental Safety Systems, Inc., 1997a). The DST test block was characterized prior to the onset of heating. On-site characterization of the local geology, *in situ* hydrology, and local rock mass quality was supplemented with laboratory tests of thermal-hydrological-mechanical-chemical properties. Characterization data collected from the single-heater test (SHT) block (Tsang et al., 1999; Blair et al., 1998) were also incorporated. The ensemble of these data provides the characterization of the DST block and model parameters and is consistent with results from previous nonthermal test studies by Brechtel et al. (1995) and TRW Environmental Safety Systems, Inc. (1997a). The data are also consistent with parameter values cited in the Total System Performance Assessment–Viability Assessment (TSPA-VA) (TRW Environmental Safety Systems, Inc., 1998a).

The primary components of Alcove 5 indicated in figure 4-2 [also taken from TRW Environmental Safety Systems, Inc. (1997a)] are the site of the SHT (known as the thermomechanical alcove), the observation drift, the connecting drift, and the heated drift. A plan-view schematic of the relative placement of the heated drift to the observation drift is shown in figure 4-1. The 5-m-diameter, 47.5-m-long heated drift is closed at the east end by a thermal bulkhead. Approximately 12 m of the west end of the heated drift is lined with cast-in-place concrete ground support. Concrete inverts were placed along the entire floor of the heated drift to provide a flat surface. Thermal sources for the heated drift consist of nine canister heaters, placed end to end on the floor of the heated drift, and 50 wing heaters (25 on either side), emplaced in horizontal boreholes drilled into the sidewalls of the heated drift about 0.25 m below the springline. The wing heaters are spaced 1.83 m apart. Each wing heater has two segments, both 5 m long, with a larger power output from the outer segment. The inner wing heater segment is separated from the heated drift by a space of 1.5 m.

## 4.1 DRIFT-SCALE HEATER TEST MODEL DOMAIN

A vertically oriented two-dimensional cross section was assembled for this analysis of the DST. The cross section intersects the axis of the heater drift mid-distance between the bulkhead and the terminus of the heated drift. The modeled area extends 200 m in the vertical direction and 160 m in the horizontal direction with the center of the heated drift placed at the center of the numerical model. The model is represented using an unstructured grid loosely patterned after the grid of Birkholzer and Tsang (1997). The full grid, 1,744 nodes, is illustrated in figure 4-3, and a close up view of the grid in the vicinity of the heated drift is shown in figure 4-4, which illustrates the finer mesh resolution in areas expected to experience large temperature, saturation, and pressure gradients. Future simulation of the DST includes an evaluation of the effect of the Observation Drift on the DST block. Using the grid for this and other nonsymmetric types of evaluations precluded modeling only half the domain with respect to a vertical plane of symmetry. Three hydrostratigraphic units were included in the model: Tptpul (TSw33), Tptpmn (TSw34), and Tptpll (TSw35) of the Topopah Spring welded unit. The thickness of the Tptpmn in the vicinity of Alcove 5 is approximately 35 m, with the centerline of the heated drift approximately 24 m below the base of the Tptpul (TRW Environmental Safety Systems, Inc., 1997b).

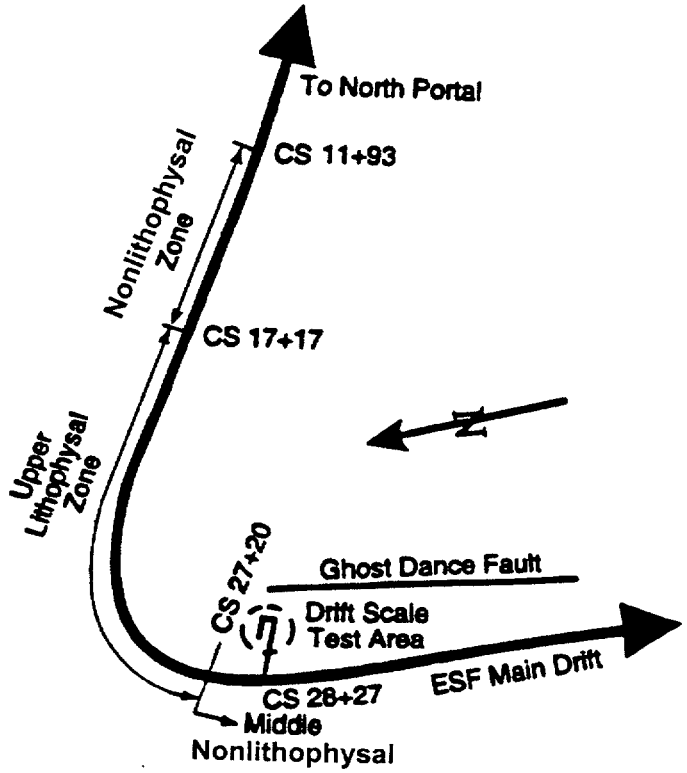


(a) Plan View

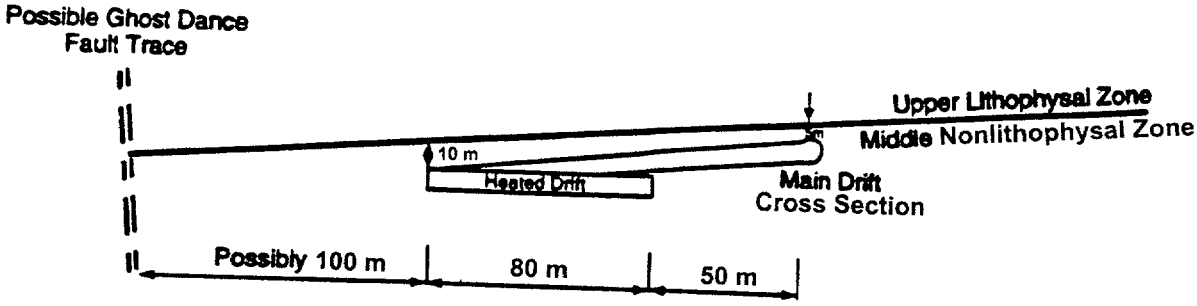


Reference Only
(SCALE APPROXIMATE)

(b) Profile View

**Figure 4-1. (a) Plan view at the North Ramp of the Exploratory Studies Facility and Drift-Scale Test area, (b) cross section of the Drift-Scale Test area showing the heated drift in relation to the main drift and contact between geological units (TRW Environmental Safety Systems, Inc., 1997a)**

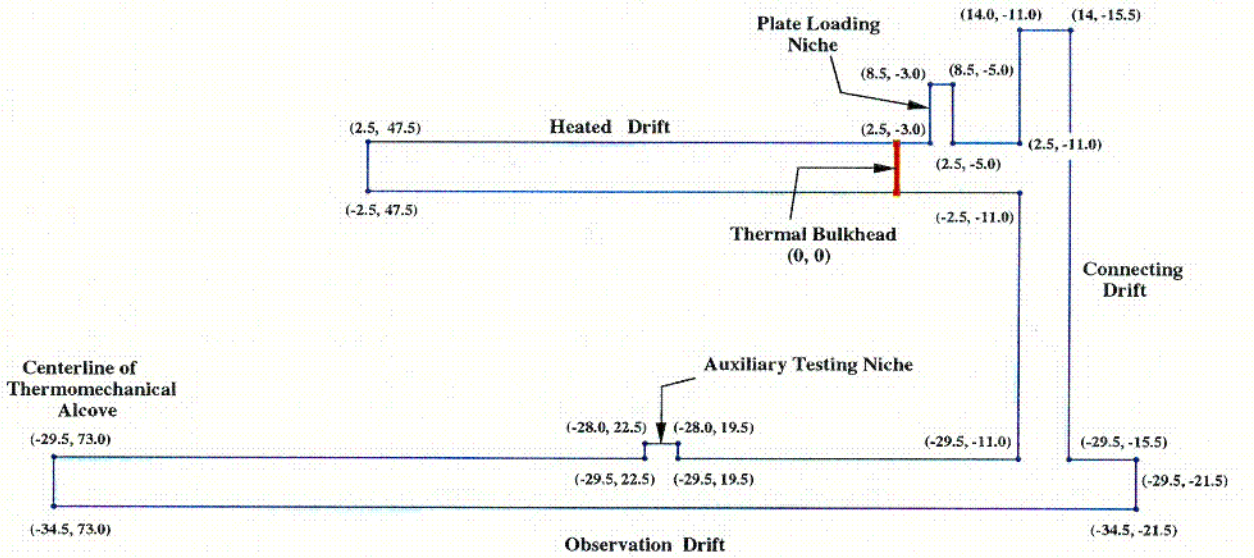


Notes:
1. X and Y coordinates are given in meters.
2. Z coordinates (vertical) are not included.
3. Only key locations are provided.
4. Coordinates are based on design with the following as-builts tolerances:
   Horizontal alignment = - 0 to + 0.5m
   All other = - 0 to + 0.3m

0 5 10
(meters)

**Figure 4-2. Plan view schematic of the primary components of Alcove 5 and the Drift-Scale Heater Test region (TRW Environmental Safety Systems, Inc., 1997b)**



C01

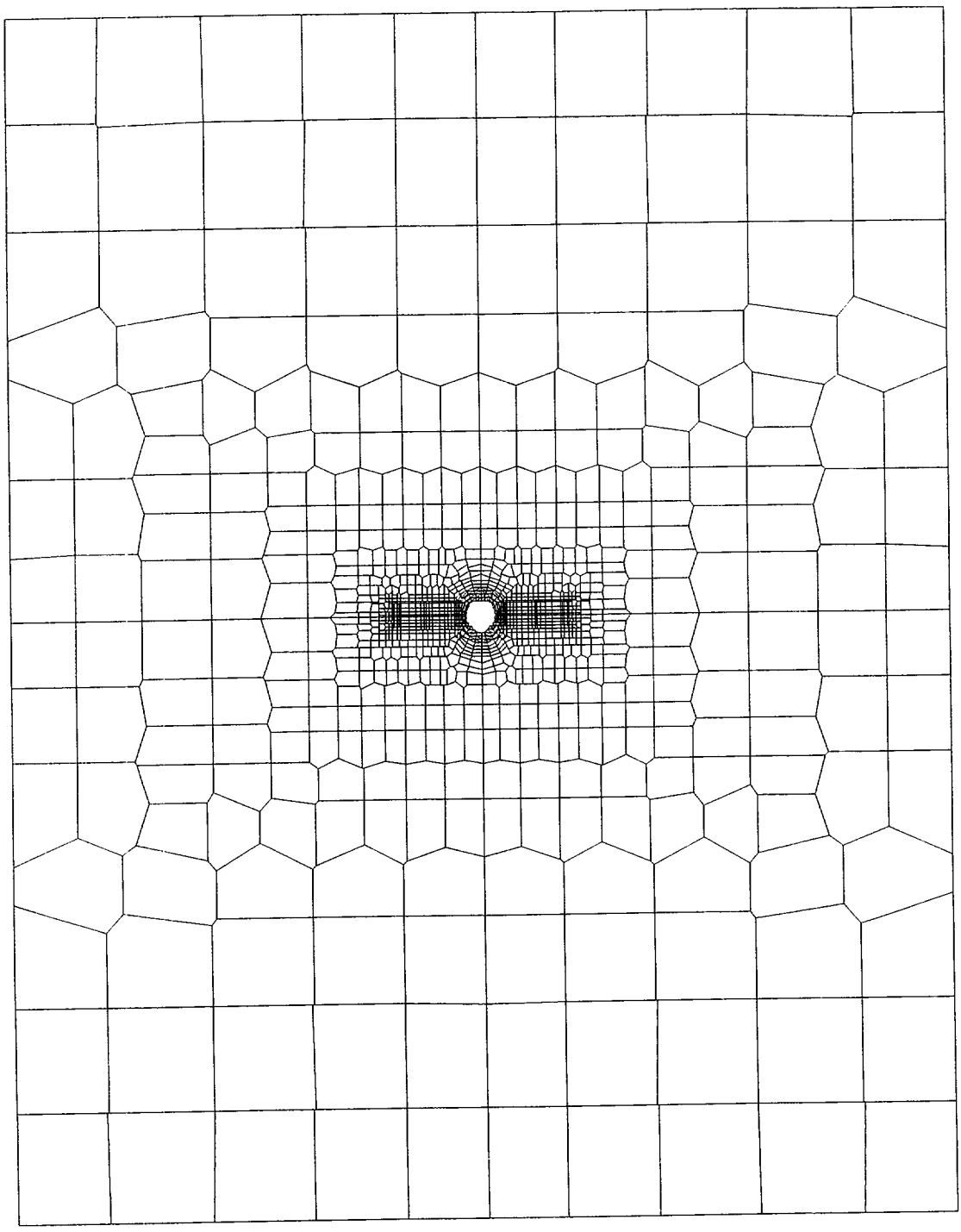

**Figure 4-3. Unstructured vertically oriented, two-dimensional grid discretization of the Drift-Scale Heater Test**

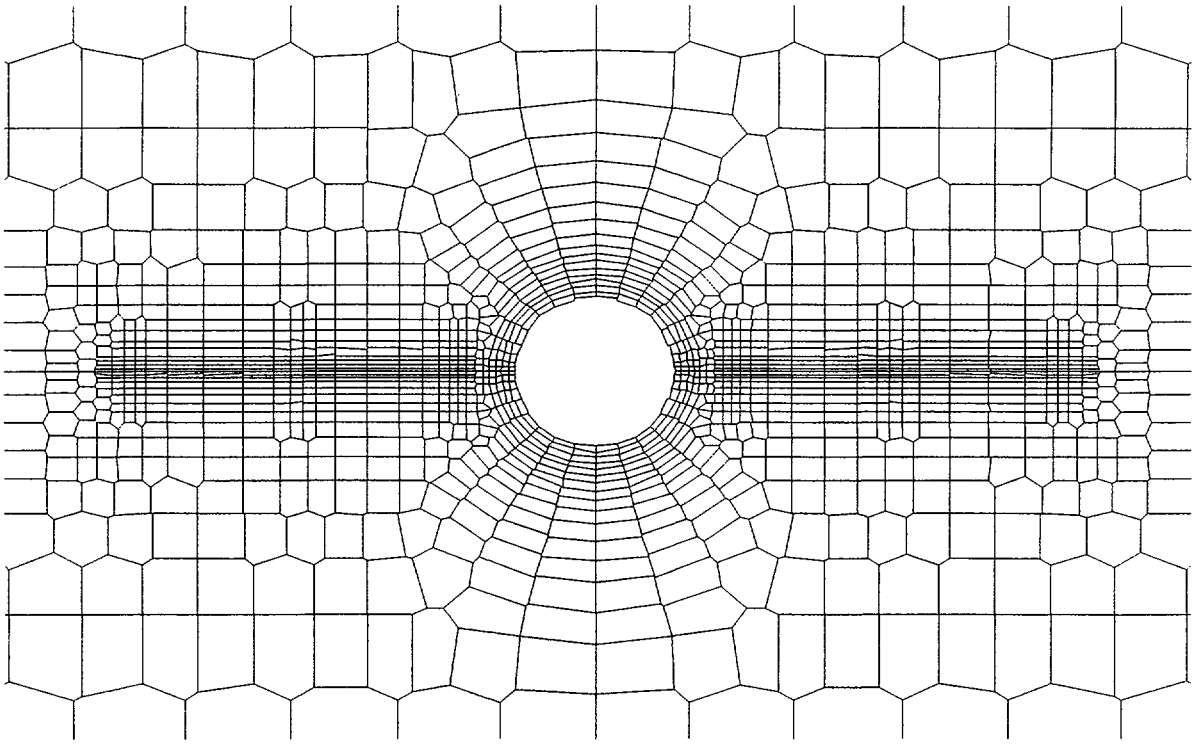

**Figure 4-4. Closeup view of drift-scale model discretization**

## 4.2 MODEL PROPERTY ASSIGNMENT

Property values for the three hydrostratigraphic units of the DST model, the TSw33, TSw34, and TSw35, were taken from the TSPA-VA (TRW Environmental Safety Systems Inc., 1998a). The particular values from the TSPA-VA used in this study were taken from the TH parameter set calibrated against the SHT. These values are summarized in tables 4-1 through 4-3.

**Table 4-1. Matrix hydraulic properties taken from Total System Performance Assessment–Viability Assessment thermal-hydrological parameter set (TRW Environmental Safety Systems Inc., 1998a)**

| Unit | Porosity | Permeability ($m^2$) | $S_r$ | $\alpha$ ($Pa^{-1}$) | m |
|---|---|---|---|---|---|
| TSw33 | 0.135 | $2.04 \times 10^{-17}$ | 0.06 | $6.21 \times 10^{-6}$ | 0.2479 |
| TSw34 | 0.089 | $4.08 \times 10^{-18}$ | 0.18 | $1.19 \times 10^{-6}$ | 0.3212 |
| TSw35 | 0.115 | $2.22 \times 10^{-17}$ | 0.08 | $4.01 \times 10^{-6}$ | 0.1983 |

**Table 4-2. Fracture hydraulic properties from Total System Performance Assessment–Viability Assessment thermal-hydrological parameter set (TRW Environmental Safety Systems Inc., 1998a)**

| Unit | Porosity | Permeability Vertical ($m^2$) | Permeability Horizontal ($m^2$) | $S_r$ | $\alpha$ ($Pa^{-1}$) | m |
|---|---|---|---|---|---|---|
| TSw33 | $1.05 \times 10^{-4}$ | $2.63 \times 10^{-11}$ | $8.91 \times 10^{-13}$ | 0.01 | $1.73 \times 10^{-3}$ | 0.667 |
| TSw34 | $1.24 \times 10^{-4}$ | $6.76 \times 10^{-12}$ | $4.27 \times 10^{-13}$ | 0.01 | $9.34 \times 10^{-4}$ | 0.643 |
| TSw35 | $3.29 \times 10^{-4}$ | $3.80 \times 10^{-12}$ | $9.12 \times 10^{-13}$ | 0.01 | $1.26 \times 10^{-3}$ | 0.667 |

**Table 4-3. Matrix thermal and physical properties [from Total System Performance Assessment–Viability Assessment (TRW Environmental Safety Systems Inc., 1998a)]**

| Unit | Thermal Conductivity–Dry (W/m-K) | Thermal Conductivity–Wet (W/m-K) | Rock-Specific Heat (J/kg-K) | Rock Density ($kg/m^3$) |
|---|---|---|---|---|
| TSw33 | 0.71 | 1.80 | 883 | 2510 |
| TSw34 | 1.56 | 2.33 | 948 | 2530 |
| TSw35 | 1.20 | 2.02 | 900 | 2540 |

## 4.3 BOUNDARY CONDITIONS

The vertical boundaries of the model were specified as adiabatic with no fluid flow. The top boundary for the basecase was specified as a mixed boundary with specified flux, and the bottom boundary was specified as a Dirichlet type with prescribed pressure, temperature, and saturation. The mixed boundary condition at the top allows gas and heat transport in or out of the model while maintaining pressure and temperature as specified. The heater drift was not explicitly included in the model; instead, the heater drift wall was modeled as a no-flow boundary and heat from the floor canisters was applied directly to the heater drift walls. The effect of the no-flow boundary at the heater drift wall on the predicted ambient saturation is assumed to be minimal, except perhaps in the near field below the drift. The wing heaters have the same hydraulic properties as the adjoining rock (Tptpmn) and should not affect ambient saturation predictions.

The temperature was specified as 22 and 26 °C at the top and bottom boundaries for a geothermal gradient of 0.02 °C/m and a temperature of 24 °C at the DST horizon. A static gas pressure difference of 2,156 Pa between the top and bottom boundaries was specified to avoid imposing an unrealistic external gas gradient. This pressure is equivalent to a 200-m tall column of air at standard pressure and temperature. Gas pressures of 89,156 Pa at the bottom and 87,000 Pa at the top give a gas pressure at the DST horizon of slightly less than 88,000 Pa, consistent with observed gas pressures (Bodvarsson and Bandurraga, 1997).

## 4.4 INITIAL CONDITIONS

Sensitivity analyses conducted in a previous study evaluated how different property assignments and boundary and initial conditions affect pre-DST ambient matrix saturation and predictions of heat and mass transfer during the heating phase of the DST (Green et al., 2000). The sensitivity analyses were accomplished in a progression of steps. First, ambient saturation was determined by simulating flow in the absence of heat at the DST for sufficiently long periods of time that steady-state flow conditions were approximated. Steady-state flow conditions were usually approximated in 300,000–700,000 yr, although steady state was approximated in as little as 100,000 yr for models with reduced fracture permeability. Sensitivity analyses were performed for a model assigned with basecase property values, except for the variable being investigated. The basecase property values used in these analyses are shown in tables 4-1 through 4-3. Ambient matrix saturation was selected as the key state variable to evaluate the appropriateness of the pretest conditions for the conceptual and numerical models used to simulate the DST. This selection was made because of the sensitivity of saturation to changes in model design and the ability to measure matrix saturation on core and grab samples collected at the site. Ambient matrix saturation for TSw34 is documented as 0.924 in the Thermal Tests Thermal-Hydrological Analysis Model Report (TRW Environmental Safety Systems, Inc., 2000).

Second, transient heat and mass transfer were predicted for the heating phase of the DST using the predicted ambient conditions as the initial conditions. Included in these transport analyses were simulations conducted to evaluate the effect of lower fracture permeability, higher thermal conductivity in the host rock, variations in the infiltration rate, and the potential effect of mass loss through the DST thermal bulkhead.

Ambient matrix saturation was predicted for a range of several different model parameters values in a previous investigation (Green et al., 2000). Model parameters evaluated in this previous study were infiltration rate, block size, liquid flow from matrix to fracture interaction area (i.e., $A^*_{mod}$), the upper boundary condition, and fracture permeability. These parameters were selected for investigation because sensitivity analysis results indicated that changes in these property values have a significant effect on predicted matrix saturation. Specific changes to model parameters evaluated were

- surface boundary changed from Neumann to mixed
- block size varied 0.25–20 m; infiltration flux at the surface varied from 0.00036 mm/yr to 3.6 mm/yr
- liquid flow from matrix to fracture interaction area varied from 1.0 to 1.23 $\times 10^{-3}$ in the TSw34 and from 1.0 to 5.0 $\times 10^{-4}$ in the TSw33 and TSw35, and
- anisotropic fracture permeability decreased by three orders of magnitude in the x-, y-, and z-directions from the basecase values

As demonstrated in the investigation by Green et al. (2000), changes in block size, infiltration rate, and surface boundary condition proved to have a significant effect on ambient matrix saturation. Variation in $A^*_{mod}$ had negligible effect on ambient matrix saturation in these simulations. Changes in values assigned to fracture permeability had negligible effect on ambient matrix saturation, but did affect temperatures and saturations predicted for the heating phase of the DST.

A modified set of basecase properties was identified for analysis in this report based on the results of Green et al. (2000). Fracture permeability and thermal conductivity were modified from property values specified in tables 4-1 through 4-3. Fracture permeabilities for all three model units were uniformly reduced by a factor of 1,000. As discussed in Green et al. (2000), although changes in fracture permeability values had minimal effect on ambient saturations, a reduction in fracture permeability was required to reduce the presence of a prominent heat pipe that was predicted over the heater drift using basecase property values, but was not observed at the DST. The revised fracture permeability values are presented in table 4-4.

**Table 4-4. Modified values assigned to fracture permeability**

| Unit | Vertical Permeability ($m^2$) | Horizontal Permeability ($m^2$) |
|---|---|---|
| TSw33 | $2.63 \times 10^{-13}$ | $8.91 \times 10^{-16}$ |
| TSw34 | $1.24 \times 10^{-15}$ | $4.27 \times 10^{-16}$ |
| TSw35 | $3.80 \times 10^{-15}$ | $9.12 \times 10^{-16}$ |

In similar fashion, thermal conductivity was modified in simulations for the heating phase of the DST. A uniform decrease of 20 percent in the values assigned to thermal conductivity was evaluated (table 4-5). These values are considered reasonable modifications to account for differences between solid, intact matrix samples measured in the laboratory and the fractured rock encountered at the test site.

**Table 4-5. Basecase and modified values assigned to thermal conductivity [W/(m-K)]**

| Unit | TSw33 (Tptpul) | | TSw34 (Tptpmn) | | TSw35 (Tptpll) | |
|---|---|---|---|---|---|---|
| Saturation | Dry | Wet | Dry | Wet | Dry | Wet |
| Basecase | 0.71 | 1.80 | 1.56 | 2.33 | 1.20 | 2.02 |
| Modified | 0.57 | 1.44 | 1.25 | 1.86 | 0.96 | 1.62 |

An infiltration rate of 0.10 mm/yr into the fracture continuum at the top boundary was specified in these analyses. A saturation of 0.917 was predicted for this rate of infiltration for the reference point located in the TSw34, 8.9 m directly above the heater drift center. The predicted value of 0.917 is sufficiently close to the value of 0.924 observed at the DST (TRW Environmental Safety Systems, Inc., 2000). It should be noted that other combinations of property values and boundary conditions also predict reasonable ambient matrix saturations. This ambiguity suggests that predicting an appropriate ambient saturation using a particular model does not in itself assure that the model is an appropriate, or even acceptable, representation of the DST. The ability to predict matrix saturations consistent with the published values does not provide conclusive evidence that either the conceptual model is appropriate for the test case or that assigned model input values are inappropriate. Additionally, the question remains whether the documented ambient saturation values are representative of the DST environment. All three possibilities should be examined in future evaluations.

## 4.5 MODEL HEAT SOURCE

Heat was introduced into the model at the heated drift and at the inner outer wing heaters. The heated drift cavity was not explicitly included in the model because of difficulties associated with representing the air space within the drift, radiative and convective heat transfer between the heater canisters and the drift wall, and the physics of heat and mass transfer at the drift-cavity/drift-wall boundary. The disadvantage to this simplification is that coupled TH processes at the drift wall cannot be directly or easily investigated using this model. The heat source levels were ramped up over a 4.2-hr period to the maximum heat load applied uniformly to each of the 36 drift boundary elements at the 5-m-diameter drift wall. The 50 cylindrical wing heaters were not individually represented in the numerical model, but both the inner and outer wing heaters were represented as individual rectangular slabs, thereby smearing the heat deposition in the y-direction of the model. The 4.65-m-long inner wing heater was set 1.62 m from the drift wall. The 4.45-m-long outer heater was separated from the inner heater by 0.82 m. Both wing heaters were assigned a vertical thickness of 0.2 m. These dimensions are consistent with those provided in the as-built report (TRW Environmental Safety Systems, Inc., 1998b), with the exception of the wing heater thickness. The wing heaters were modeled as 0.2 m thick, rather than the reported diameter of 24 mm, because of constraints on mesh resolution and use of two- versus three-dimensional model. Increasing the thickness of the wing heaters will distort the resulting TH regime in the region close to the heat source, however, the effect should be negligible beyond a few tens of centimeters.

The design thermal load for the DST was 68.0 kW for the canister heaters and 143.0 kW for the cumulative wing heaters (85.8 kW at the outer wing heater and 57.2 kW for the inner wing heaters) for a total of 211 kW (TRW Environmental Safety Systems, 1998c). The DST has experienced measured heat loads that deviate significantly (less) from the levels of the design heat loads since energizing in December 1997 (figure 4-5). At the time of energizing, the canister heat load was about 52.8 kW, and the cumulative wing heater heat load was about 137 kW (TRW Environmental Safety Systems, 1998d). These power levels decreased after heating started, however, the precise magnitude of decrease is not well defined. Conflicting measurements between qualified and nonqualified data suggest the heat load values decreased to between 49.4 (nonqualified) and 51.8 (qualified) kW for the canisters and between 130.8 (nonqualified) and 133.3 (qualified) kW for the wing heaters by day 179 after heating started. Qualified canister heat load measurements continued to decrease to about 51 kW by day 244, but then increased to about 53.5 kW during the next 26 d until day 270 (TRW Environmental Safety Systems, 1998b). After day 270, the canister heat load resumed a gradual, consistent decline, decreasing to 51.5 kW by day 700 (TRW Environmental Safety Systems, 1999a). The canister heat load increase from days 244 to 270 is attributed to a modification in the access drift and heat drift (outside the thermal bulkhead) ventilation system.

The wing heaters also experienced an increase in heat load soon after day 244, however, this increase followed a rather precipitous decrease in the (qualified) heater load from about 133 kW at day 185 to less than 130 kW by day 244 (TRW Environmental Safety Systems, 1998b). The cause of this precipitous heat load decrease is attributed to the loss of power to wing heater 29. Measured (qualified) heater load values continued to decrease to about 52.3 kW for the canisters and to slightly more than 130 kW for the wing heaters by day 480 (TRW Environmental Safety Systems, 1999b) and to about 51.5 kW for the canisters and 128.2 kW for the wing heaters by day 700 (TRW Environmental Safety Systems, 1999a).

Heat loads consistent with measured levels were assigned to the model in the TH evaluations.The thermal loads were ramped up to their starting power levels during a period of about 4.2 hr to avoid stability problems. Heat loads were established to resemble the (qualified) heat loads measured for the first 1.9 yr of

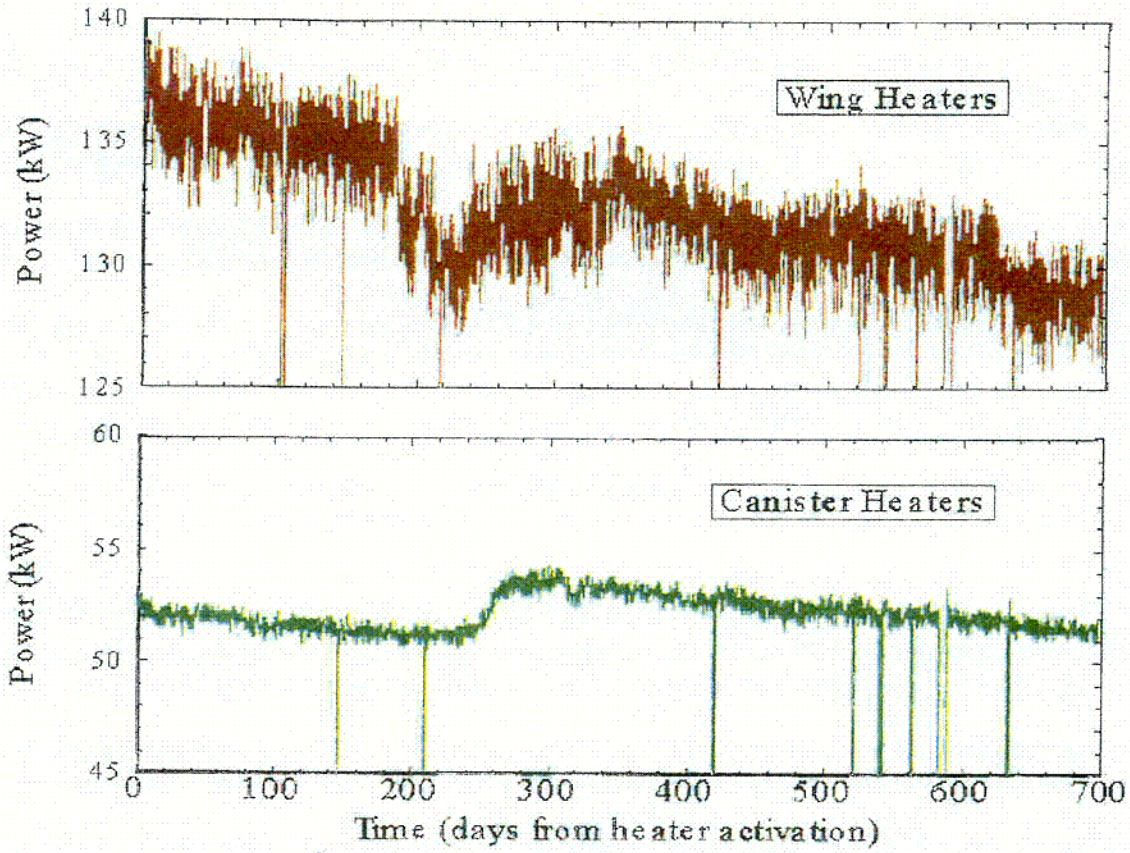


**Figure 4-5. Total power measurements ($Q$) for the wing heaters and canister heaters (TRW Environmental Safety Systems, 1999b)**

heating (TRW Environmental Safety Systems, 1999a). The measured cumulative heat load for the canister heaters was estimated to remain constant at 52.0 kW up to day 700 of the test. Transient deviations in the canister heat load from 52.0 kW, which decreased to approximately 51.0 kW about day 230 and increased to approximately 53.8 kW about day 280, were not considered in this investigation. The overall reduction in the cumulative canister heat load was 23.5 percent from the design level of 68.0 kW to the actual measured level of 52.0 kW.

The measured cumulative heat load for the wing heaters demonstrated a defined decreasing trend, with some deviation, for the first 700 d of heating. Deviations of actual heat loads from a linear decline in cumulative wing heater heat load between days 180 and 240 have been neglected and a constant linear decrease in cumulative wing heater heat load from 136.5 kW at the onset of heating to 128.2 kW at day 700 was assumed. It was also assumed that the decrease in cumulative heat load for the wing heaters occurred uniformly over both the inner and outer wing heaters. Accordingly, the inner wing heaters decreased from 54.6 to 51.3 kW and the outer wing heaters decreased from 81.9 to 76.9 kW during the first 1.9 yr of heating. The decrease in heating of the wing heaters varied from a 4.5-percent decrease from the design basecase values heat of 143.0 kW at the start of heating to a 10.3-percent decrease at day 700.



C02

## 4.6 MASS LOSS THROUGH THE THERMAL BULKHEAD

Effects from the potential loss of water through the thermal bulkhead were indirectly incorporated into the 2D model by placing mass sink terms uniformly in the elements at the drift-wall boundary. The rate of mass loss through the bulkhead has been roughly estimated to be 200 mL/hr (U.S. Nuclear Regulatory Commission, 1999).[1] The actual rate of mass loss is unknown. MULTIFLO, as currently implemented, cannot extract vapor phase water. A mass flux rate of 80 mL/hr was assigned to these test cases. Mass removal in MULTIFLO is restricted to the liquid phase. This limits the mass of water removed in the simulation to the mass of liquid water present in the heater drift-wall elements from which mass is removed. Attempts to extract water at rates in excess of 80 mL/hr failed when all liquid phase water was removed from any element. Nonetheless, the effect of the removal of limited amounts of water can be evaluated with these simulations. Heat removed from the thermal bulkhead is limited to the enthalpy associated with the removed water. The evaluation of additional sources of heat loss through the bulkhead (radiation, latent, etc.) will be conducted in future studies.

## 4.7 MODEL SIMULATIONS

Heat and mass transfer were simulated for the first year of the heating phase of the DST and compared to measured temperatures collected at the DST for the same period. Saturation at the DST is inferred using geophysical methods (i.e., electrical resistivity tomography, ground-penetrating radar, and neutron logging) for the matrix and air permeability tests for the fractures. These measurements only provide a qualitative measure of saturation at the DST. Only temperature measurements are used for comparison with simulation results at this time, although inferred saturation measurement techniques may promote a clearer interpretation of the DST.

The importance of two model factors was addressed in this comparison: the effect on model predictions from changing thermal conductivity and the effect of moisture loss through the DST thermal bulkhead. All four cases were simulated for fracture permeability values reduced by a factor of 1,000 from basecase values. The reduced fracture permeabilities were specified because they were the only property modification identified by Green et al. (2000) that effectivity minimized the formation of a heat pipe above the heater drift in the simulations. This modification was deemed necessary because only a faint expression of a heat pipe was indicated in temperature measurements taken after one year of heating at the DST. Thermal conductivity of all three model units was reduced by 20 percent because better agreement between measured and simulated temperatures was achieved compared to basecase values. Following are graphical and contour plots summarizing the DST after one year of heating. For each case, measured and simulated matrix and fracture temperature along Boreholes 158 and 160 are compared. Borehole 158 is located at the mid-point of the drift and is oriented vertically upward from the drift roof. Borehole 160 is also located at the midpoint of the heater drift, but is horizontally oriented from the springline of the heater drift toward the DST observation drift. Borehole 160 is placed about 1.0 m above the wing heaters. Both boreholes are 20 m long.

Three contour plots for each case are presented: temperature and saturation for the matrix continuum and saturation for the fracture continuum. The temperature contour plot for the fracture continuum is identical

[1]TRW Environmental Safety Systems, Inc., Interoffice correspondence memo dated October 21, 1999.

to the matrix continuum and is not included. The first simulation shows basecase values for thermal conductivity and no mass loss through the thermal bulkhead (figures 4-6a,b and figures 4-7a,b,c). The second simulation has the same property values but with a mass loss of 80 mL/hr through the thermal bulkhead (figures 4-8a,b and figures 4-9a,b,c). The third simulation has a 20-percent reduction in thermal conductivity for all three model units and no mass loss (figures 4-10a,b and figures 4-11a,b,c). The last simulation has a 20-percent reduction in thermal conductivity and a mass loss of 80 mL/hr through the thermal bulkhead (figures 4-12a,b and figures 4-13a,b,c).

Caution should be exercised in drawing conclusions from temperatures predicted near the drift wall (figures 4-6b, 4-8b, 4-10b, and 4-12b). Temperature predictions near the drift, in particular in the boundary element of the model, may be skewed because of the manner in which heat is directly applied to those elements. In general, the contour plots of predicted temperature indicate a large temperature discrepancy between the drift springline and the drift crown, with the springline temperatures being much greater. This trend is inconsistent with observed temperatures that are greater at the crown (about 190 °C) than at the springline (about 150 °C). Given the approximate method used to apply the heater drift thermal load to the numerical model, no further effort was directed to resolve temperature discrepancies to the near-drift area.

For regions beyond the drift near field (i.e., beyond the first model grid element), better agreement in temperature was achieved by reducing the thermal conductivity of the host rock units (figures 4-10a,b and figures 4-12a,b). Temperature differences in Borehole 160 (located over the wing heaters) are significantly reduced by the noted property value modification (figures 4-10b and 4-12b). Predicted temperatures in Borehole 158 (close to the heater drift crown) are increased by approximately 10 °C, reducing the difference between measured and simulated temperatures to approximately 35 °C (figures 4-10a and 4-12a). Removal of mass at a rate of 80 mL/hr uniformly from the drift wall resulted in no noticeable change in the temperature profiles predicted for Boreholes 158 and 160 (figures 4-6a,b compared to figures 4-8a,b, and figures 4-10a,b compared to figures 4-12a,b).

The simulations reported in this document consistently predicted elevated saturations in the fracture continuum. In particular, a defined zone of condensation that formed immediately beyond the boiling isotherm is predicted above the entire breadth of the heater test (figures 4-7c, 4-9c, 4-11c, and 4-13c). This condensation zone is believed to be a consequence of the reduced fracture permeability because similar results were not encountered in simulations with higher fracture permeabilities reported in Green et al. (2000). Similar to the elevated fracture saturations predicted here, the matrix was predicted to be near or at full saturation for the same zone above both the heater drift and the wing heaters (figures 4-7b, 4-9b, 4-11b, and 4-13b). The extent of elevated saturation below the heater drift was slightly greater for simulations with reduced values for thermal conductivity (figures 4-11b and 4-13b) compared to simulations using basecase property values (figures 4-7b and 4-9b).

Saturation contour plots illustrate minor changes in fracture saturation resulting from removal of mass at 80 mL/hr (figure 4-9c compared to figure 4-7c, and figure 4-13c compared to figure 4-11c). Removal at 80 mL/hr reduced the extent of elevated saturation by a couple of meters directly below the heater drift and slightly modified the shape of the elevated saturation above the heaters for simulations with a reduced thermal conductivity (figure 4-13c). Even less change occurred in the predicted saturation for the simulations with basecase values for thermal conductivity (figure 4-9c).

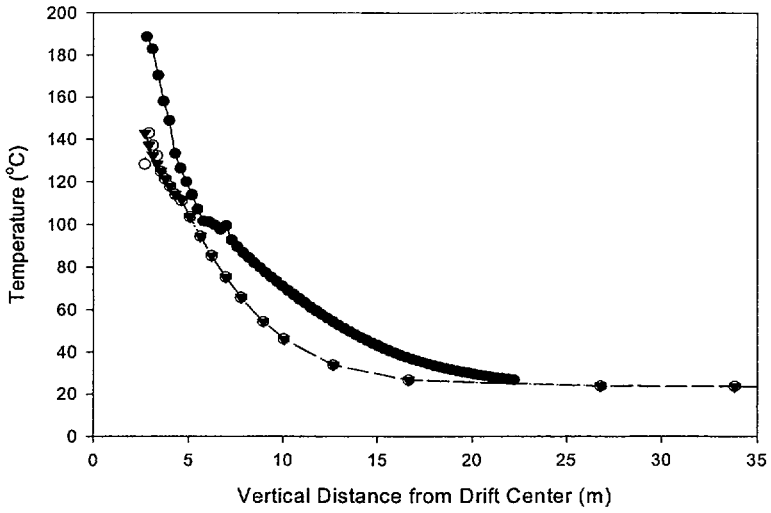


**Figure 4-6a. Comparison of measured temperatures (solid circle) versus simulated temperatures in the matrix (closed triangle) and fracture (open circle) for vertical Borehole 158 for basecase property values except for a factor of 1,000 reduction in fracture permeability**

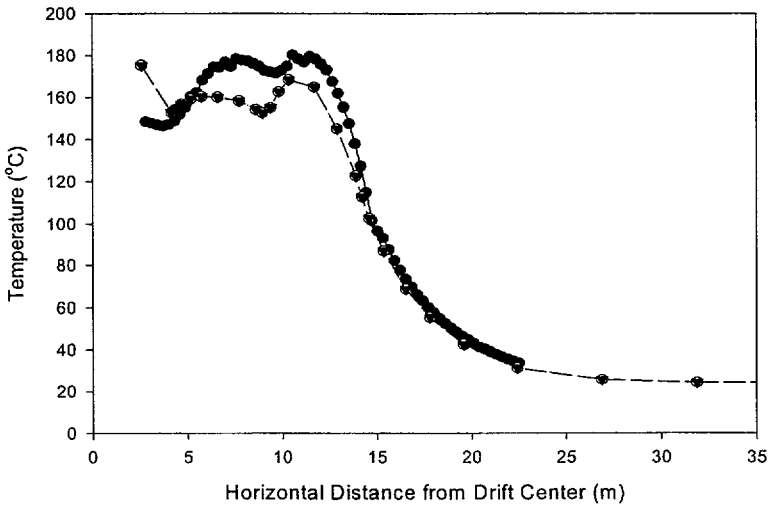


**Figure 4-6b. Comparison of measured temperatures (solid circle) versus simulated temperatures in the matrix (closed triangle) and fracture (open circle) for horizontal Borehole 160 for basecase property values except for a factor of 1,000 reduction in fracture permeability**

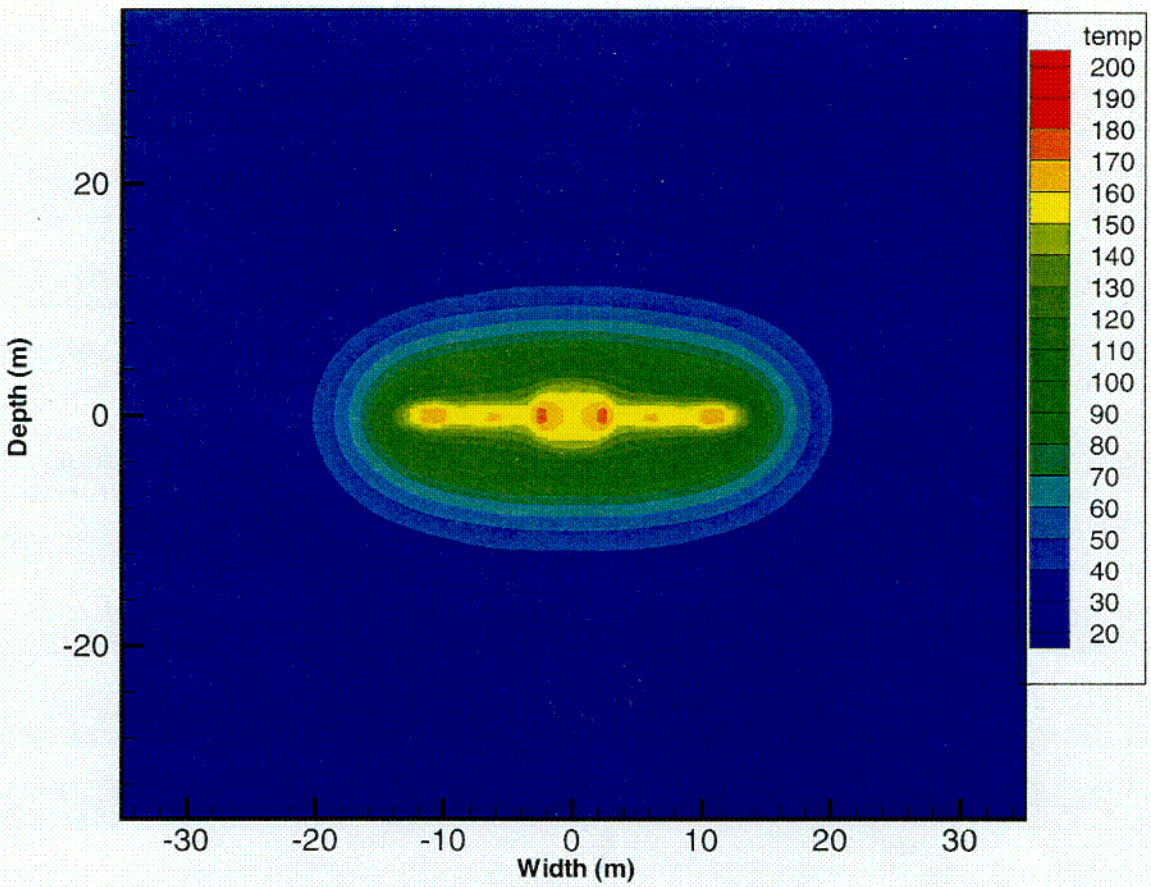


**Figure 4-7a. Contour plot of simulated matrix temperature for basecase property values except for a factor of 1,000 reduction in fracture permeability**



C03

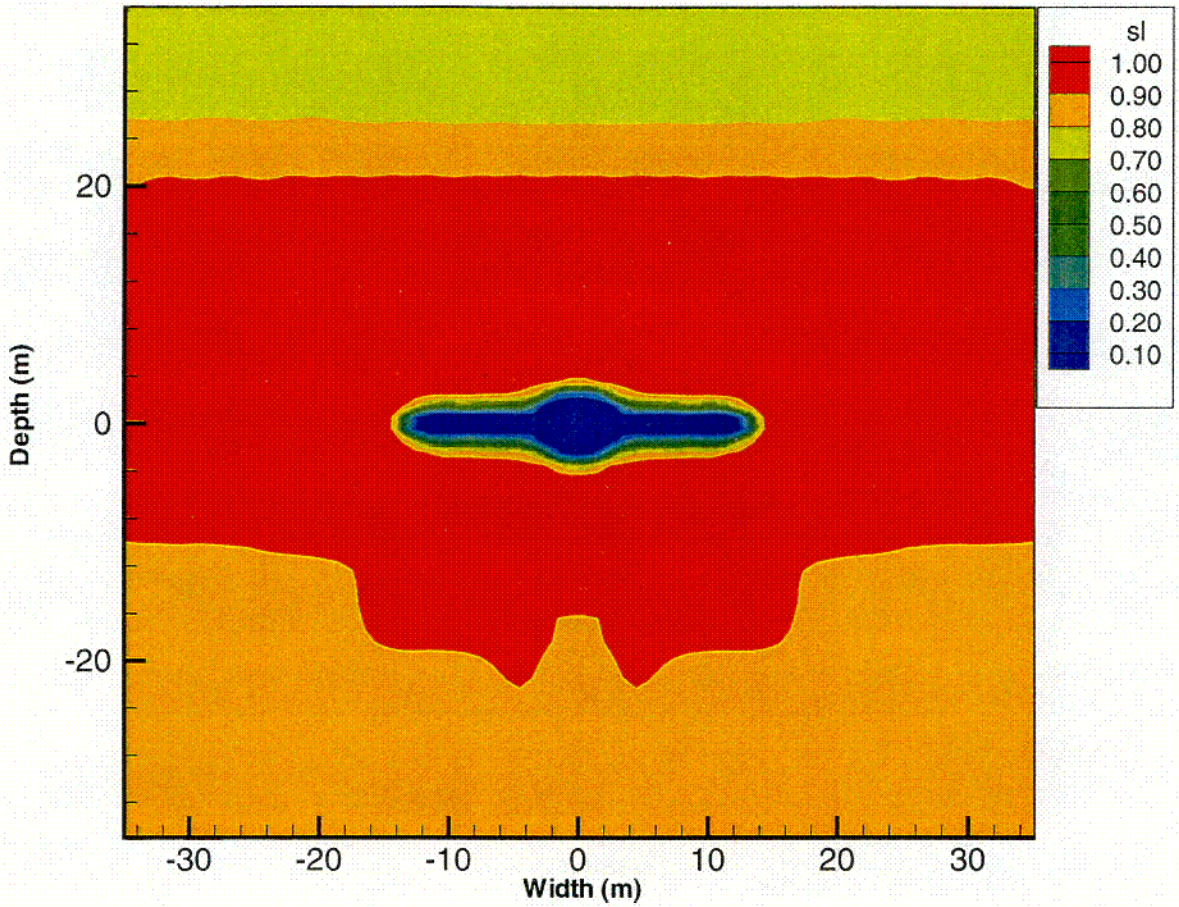


**Figure 4-7b. Contour plot of simulated matrix saturation for basecase property values except for a factor of 1,000 reduction in fracture permeability**



C04

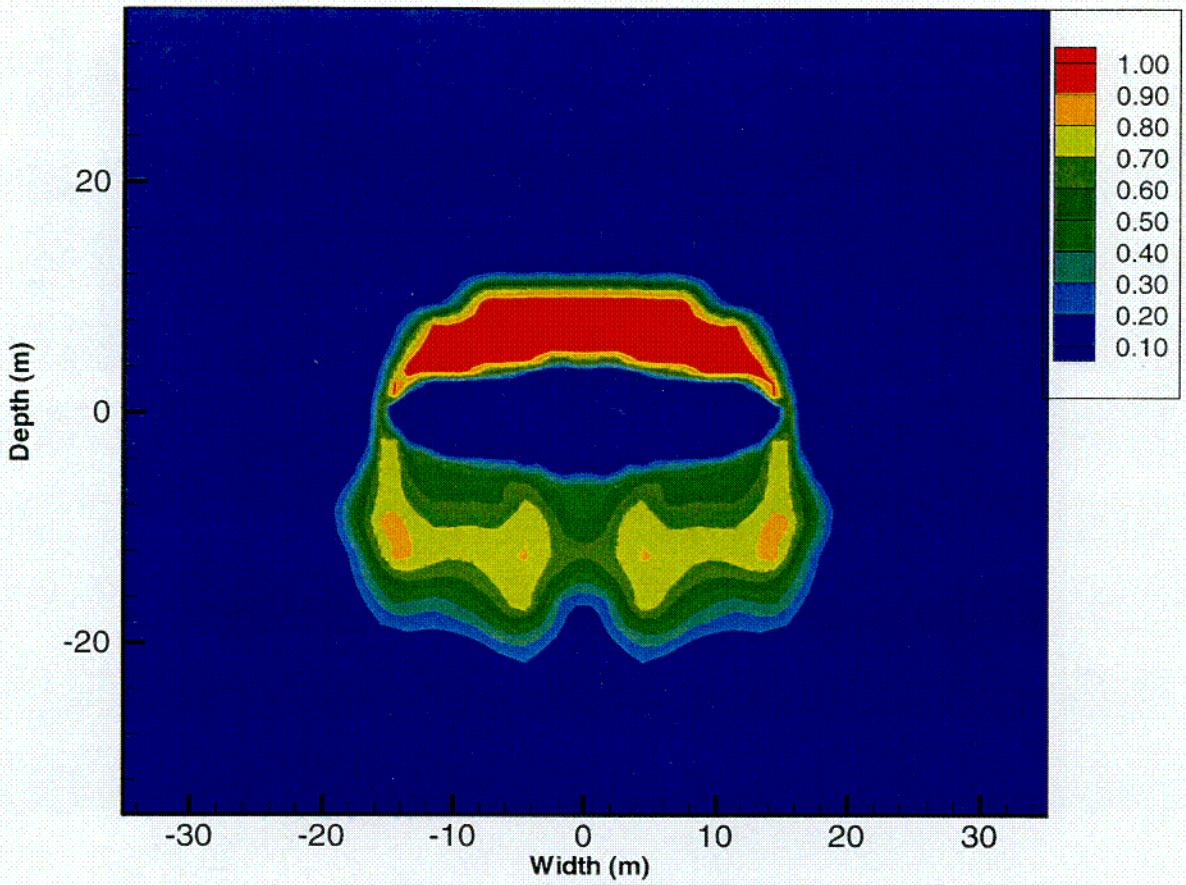


**Figure 4-7c. Contour plot of simulated fracture saturation for basecase property values except for a factor of 1,000 reduction in fracture permeability**



C05

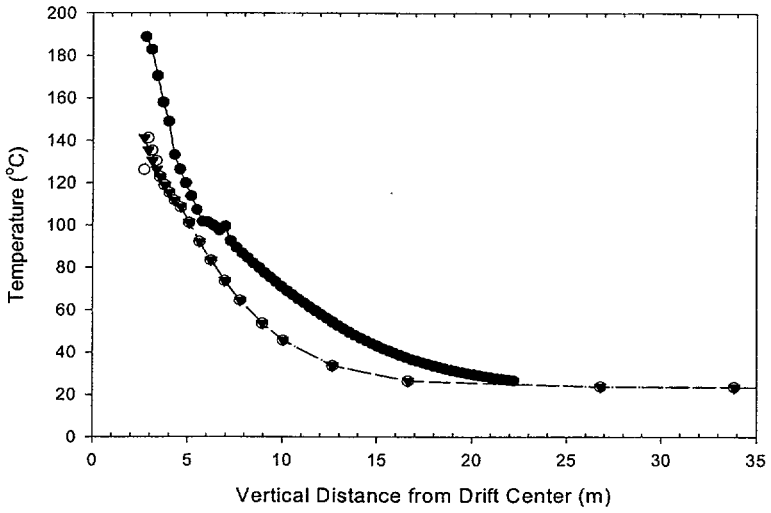


**Figure 4-8a. Comparison of measured temperatures (solid circle) versus simulated temperatures in the matrix (closed triangle) and fracture (open circle) for vertical Borehole 158 for basecase property values except for a factor of 1,000 reduction in fracture permeability and a mass loss of 80 mL/hr**

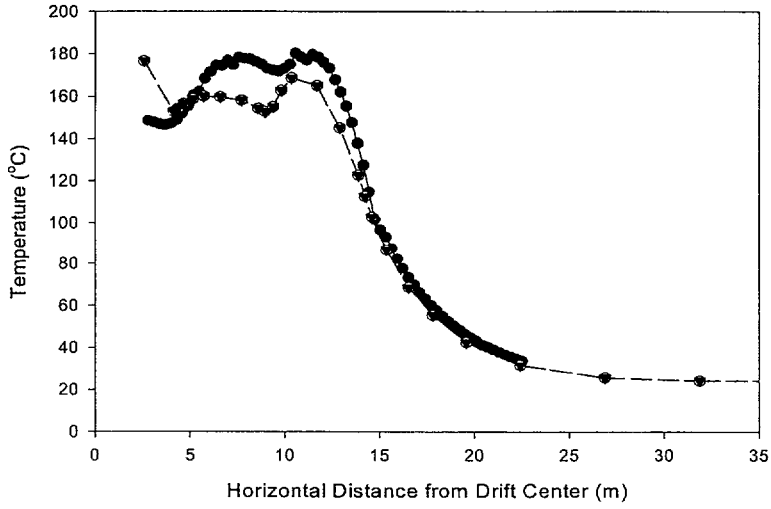


**Figure 4-8b. Comparison of measured temperatures (solid circle) versus simulated temperatures in the matrix (closed triangle) and fracture (open circle) for horizontal Borehole 160 for basecase property values except for a factor of 1,000 reduction in fracture permeability and a mass loss of 80 mL/hr**

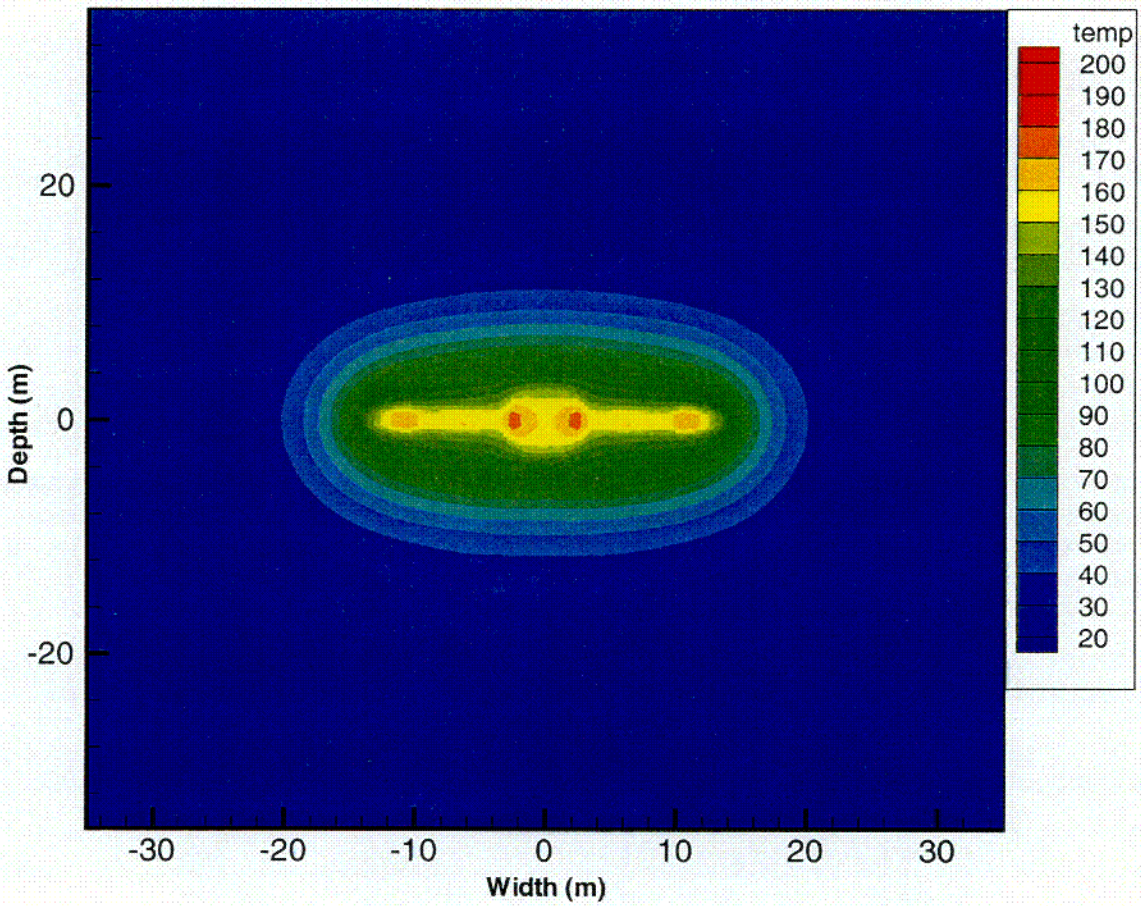


**Figure 4-9a. Contour plot of simulated matrix temperature for basecase property values except for a factor of 1,000 reduction in fracture permeability and a mass loss of 80 mL/hr**



C06

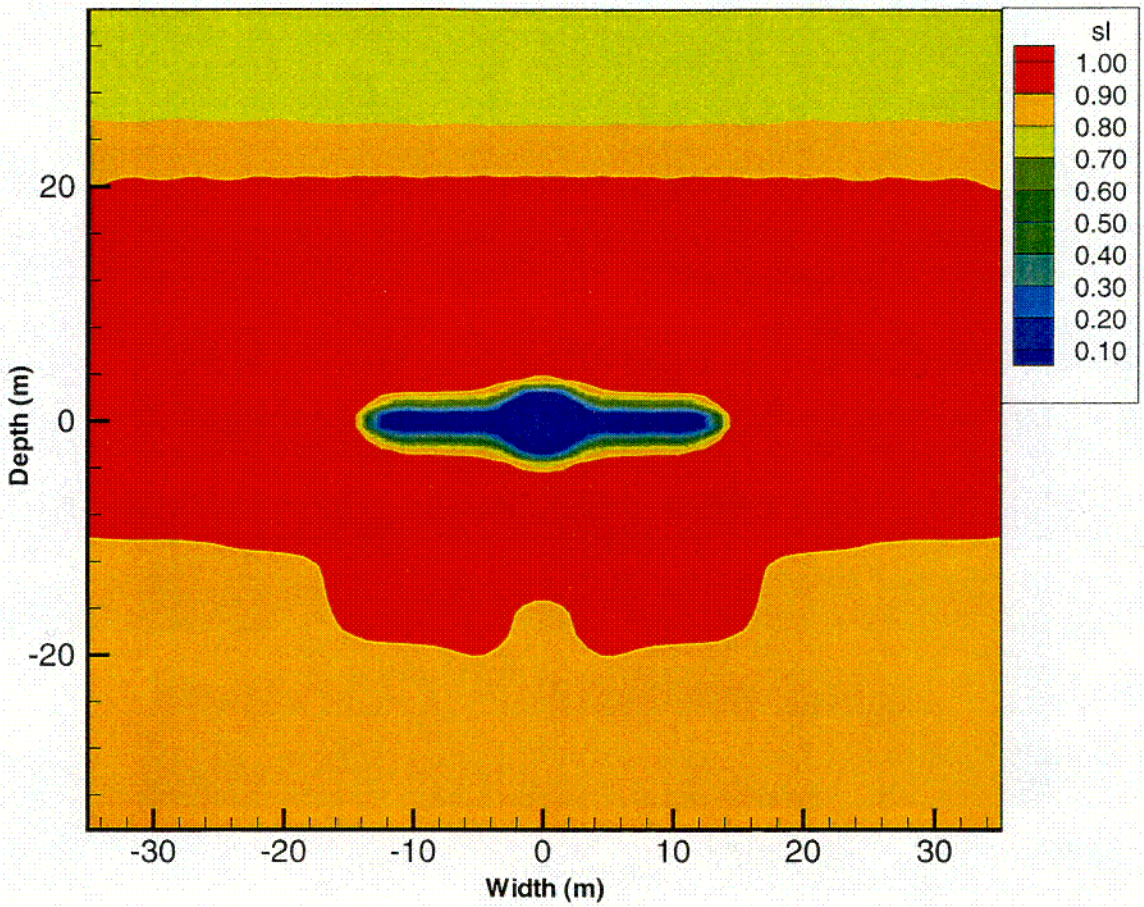


**Figure 4-9b. Contour plot of simulated matrix saturation for basecase property values except for a factor of 1,000 reduction in fracture permeability and a mass loss of 80 mL/hr**



C07

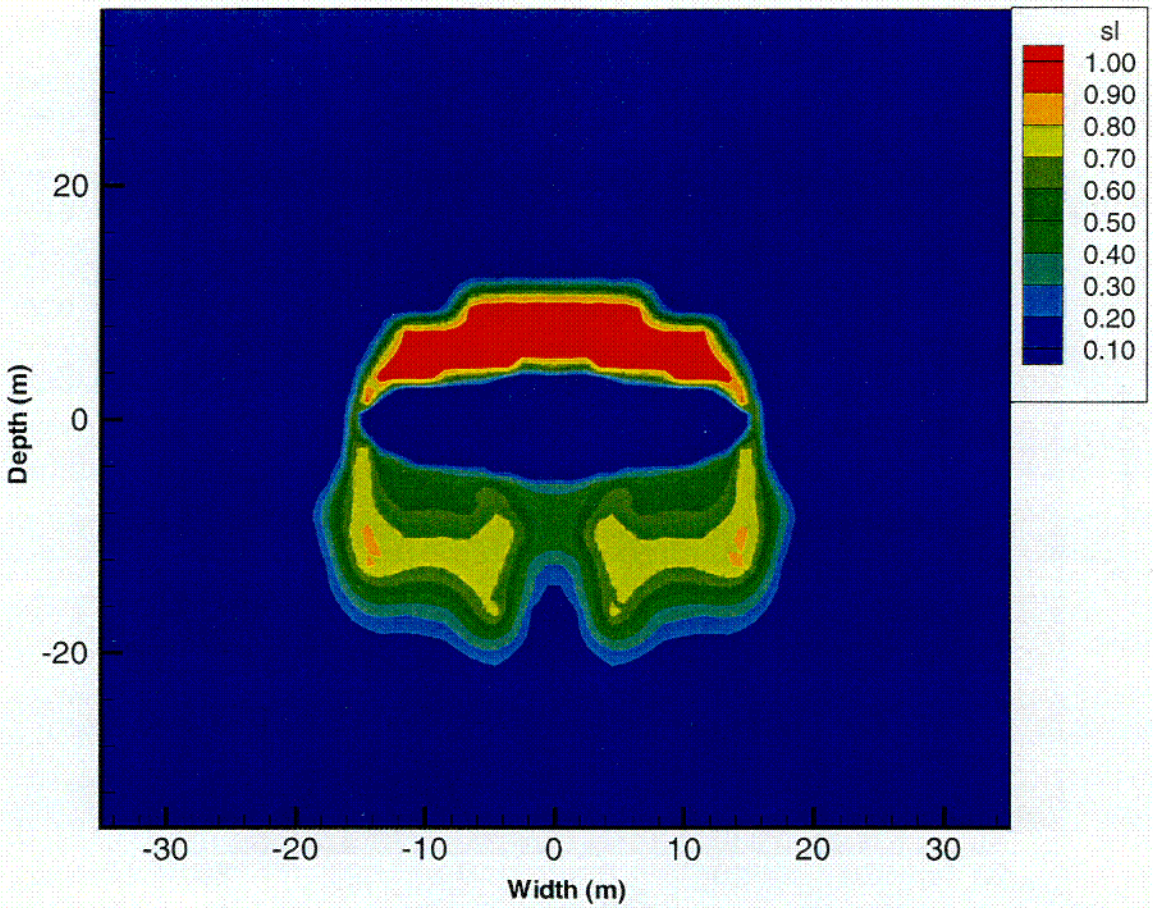


**Figure 4-9c. Contour plot of simulated fracture saturation for basecase property values except for a factor of 1,000 reduction in fracture permeability and a mass loss of 80 mL/hr**



C08

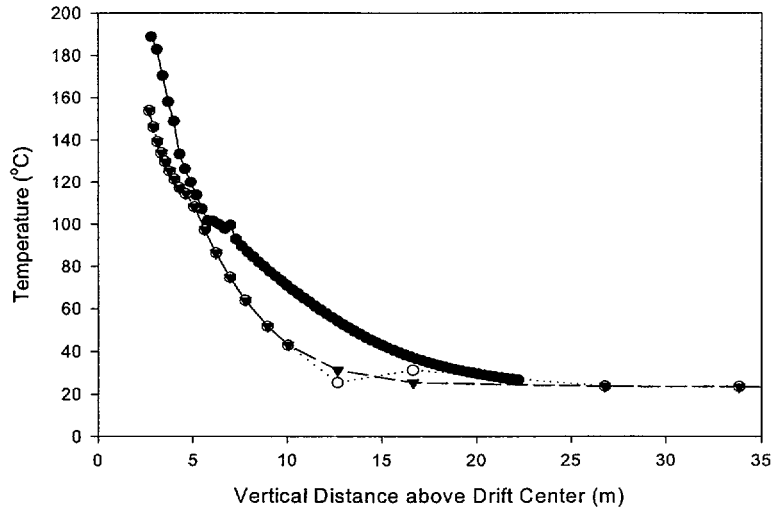


**Figure 4-10a. Comparison of measured temperatures (solid circle) versus simulated temperatures in the matrix (closed triangle) and fracture (open circle) for vertical Borehole 158 for basecase property values except for a factor of 1,000 reduction in fracture permeability and a 20-percent reduction in thermal conductivity**

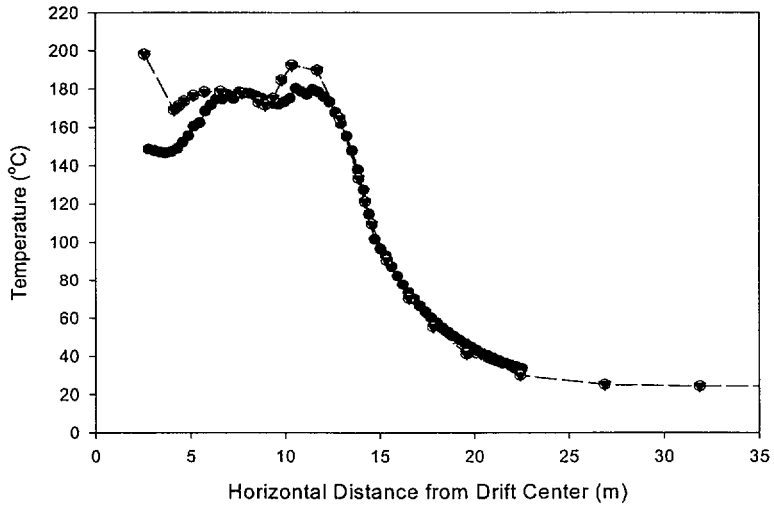


**Figure 4-10b. Comparison of measured temperatures (solid circle) versus simulated temperatures in the matrix (closed triangle) and fracture (open circle) for horizontal Borehole 160 for basecase property values except for a factor of 1,000 reduction in fracture permeability and a 20-percent reduction in thermal conductivity**

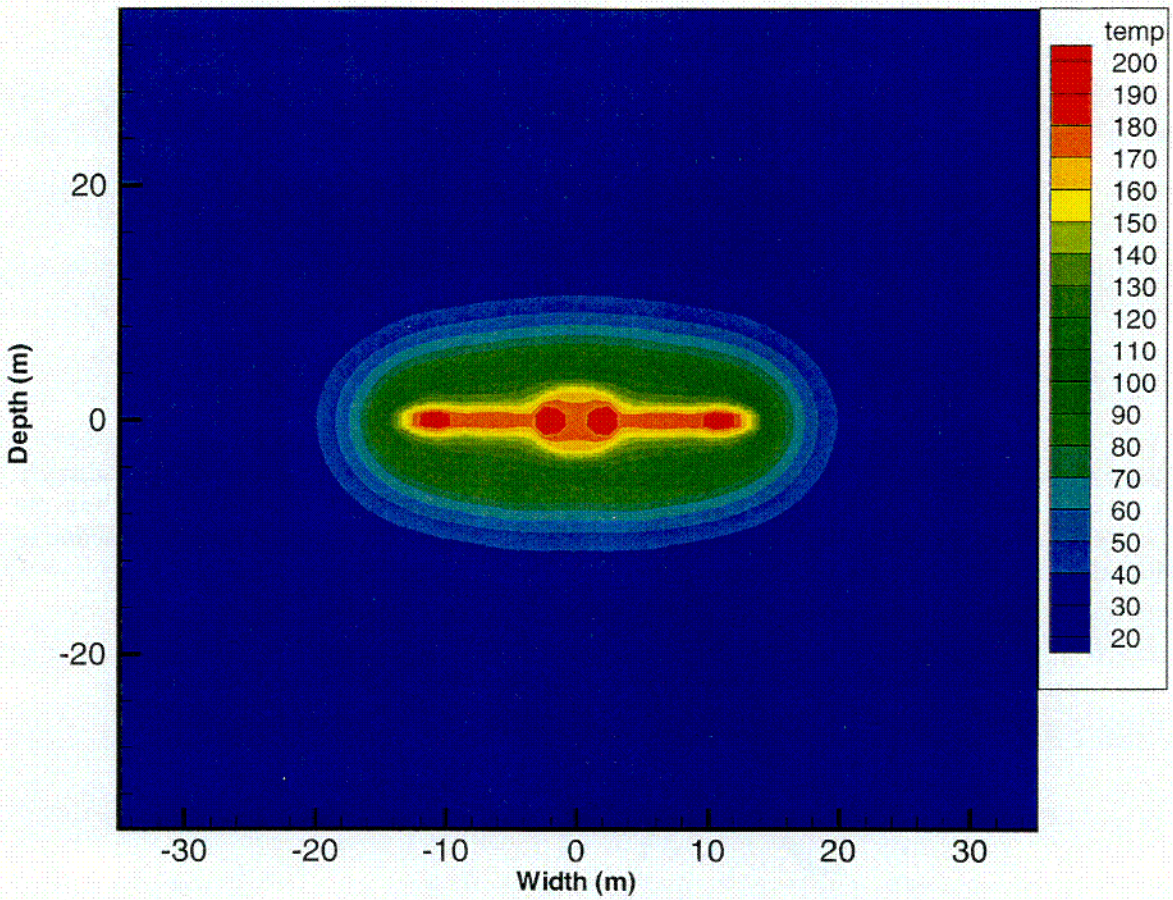


**Figure 4-11a. Contour plot of simulated matrix temperature for basecase property values except for a factor of 1,000 reduction in fracture permeability and a 20-percent reduction in thermal conductivity**



C09

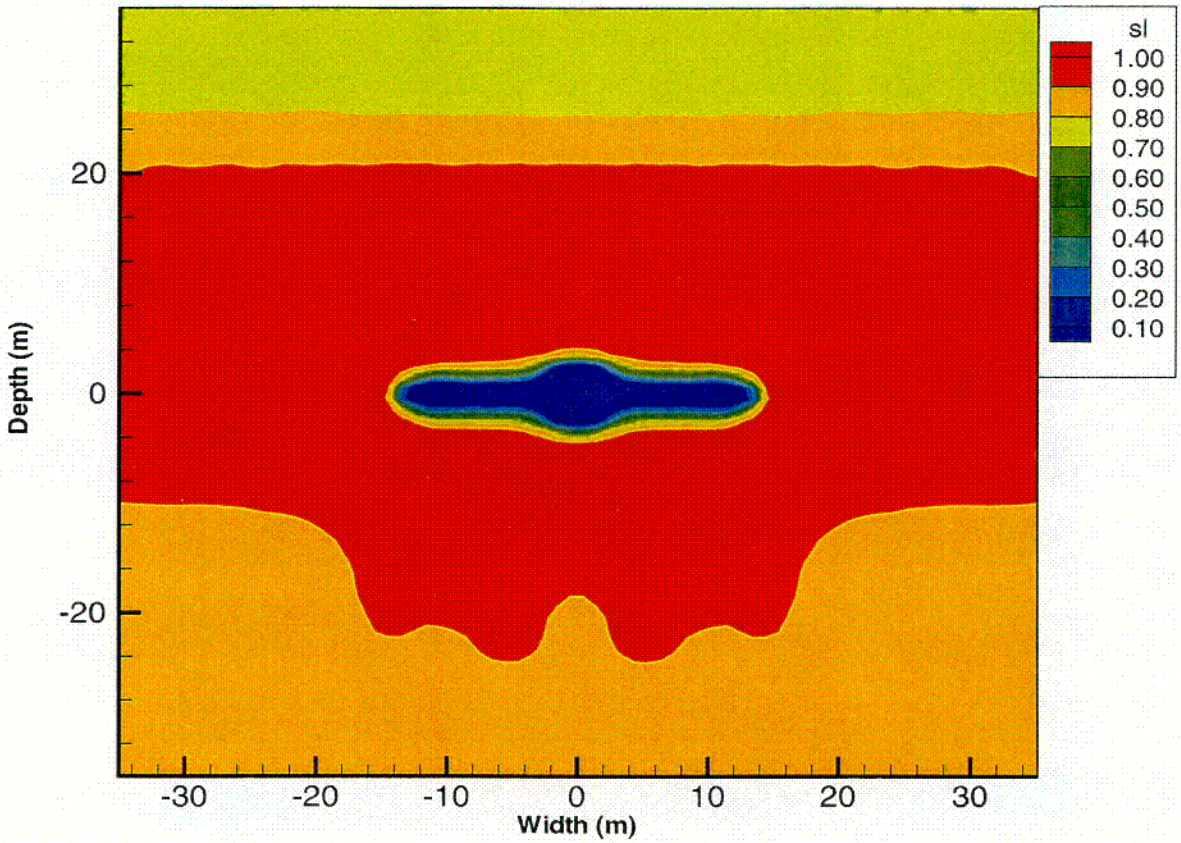


**Figure 4-11b. Contour plot of simulated matrix saturation for basecase property values except for a factor of 1,000 reduction in fracture permeability and a 20-percent reduction in thermal conductivity**



C10

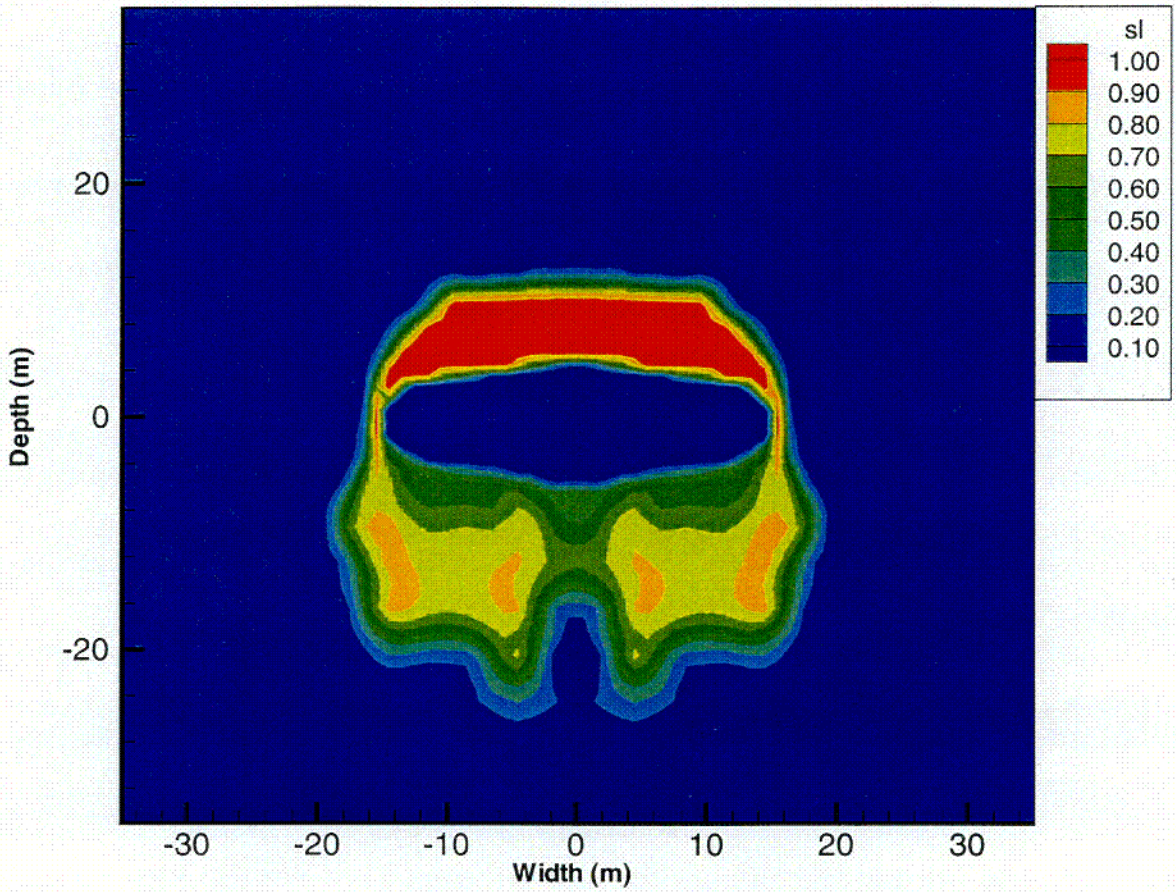


**Figure 4-11c. Contour plot of simulated fracture saturation for basecase property values except for a factor of 1,000 reduction in fracture permeability and a 20-percent reduction in thermal conductivity**



C11

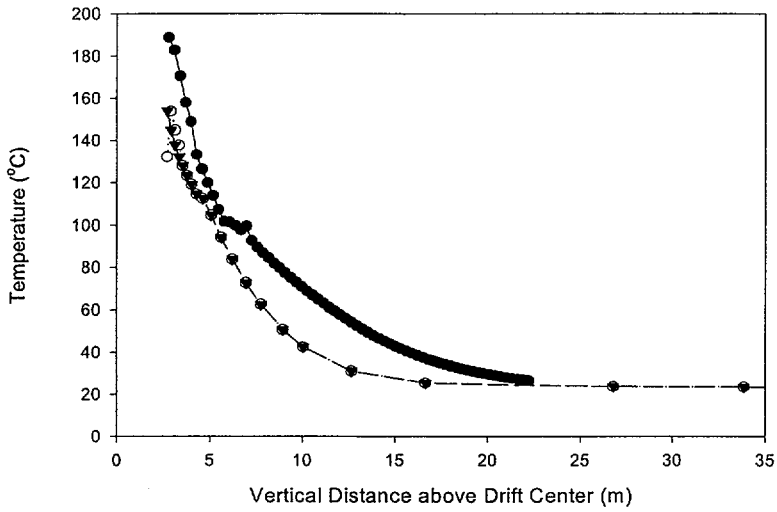


**Figure 4-12a. Comparison of measured temperatures (solid circle) versus simulated temperatures in the matrix (closed triangle) and fracture (open circle) for vertical Borehole 158 for basecase property values except for a factor of 1,000 reduction in fracture permeability, a 20-percent reduction in thermal conductivity, and a mass loss of 80 mL/hr**

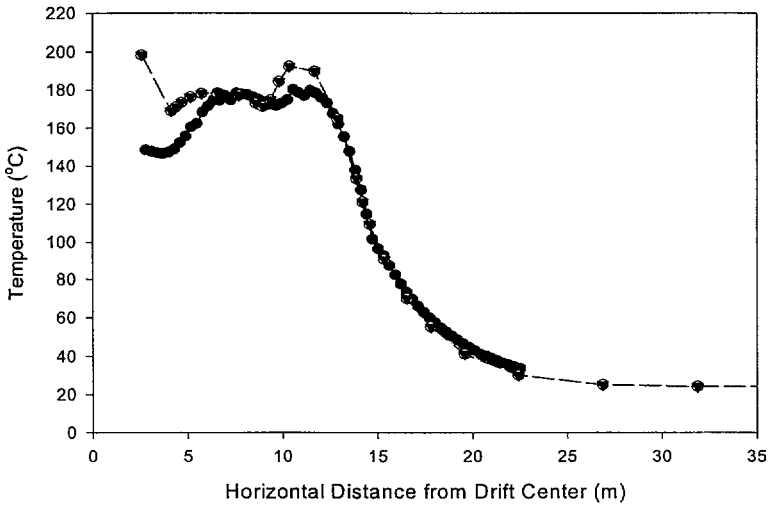


**Figure 4-12b. Comparison of measured temperatures (solid circle) versus simulated temperatures in the matrix (closed triangle) and fracture (open circle) for horizontal Borehole 160 for basecase property values except for a factor of 1,000 reduction in fracture permeability, a 20-percent reduction in thermal conductivity, and a mass loss of 80 mL/hr**

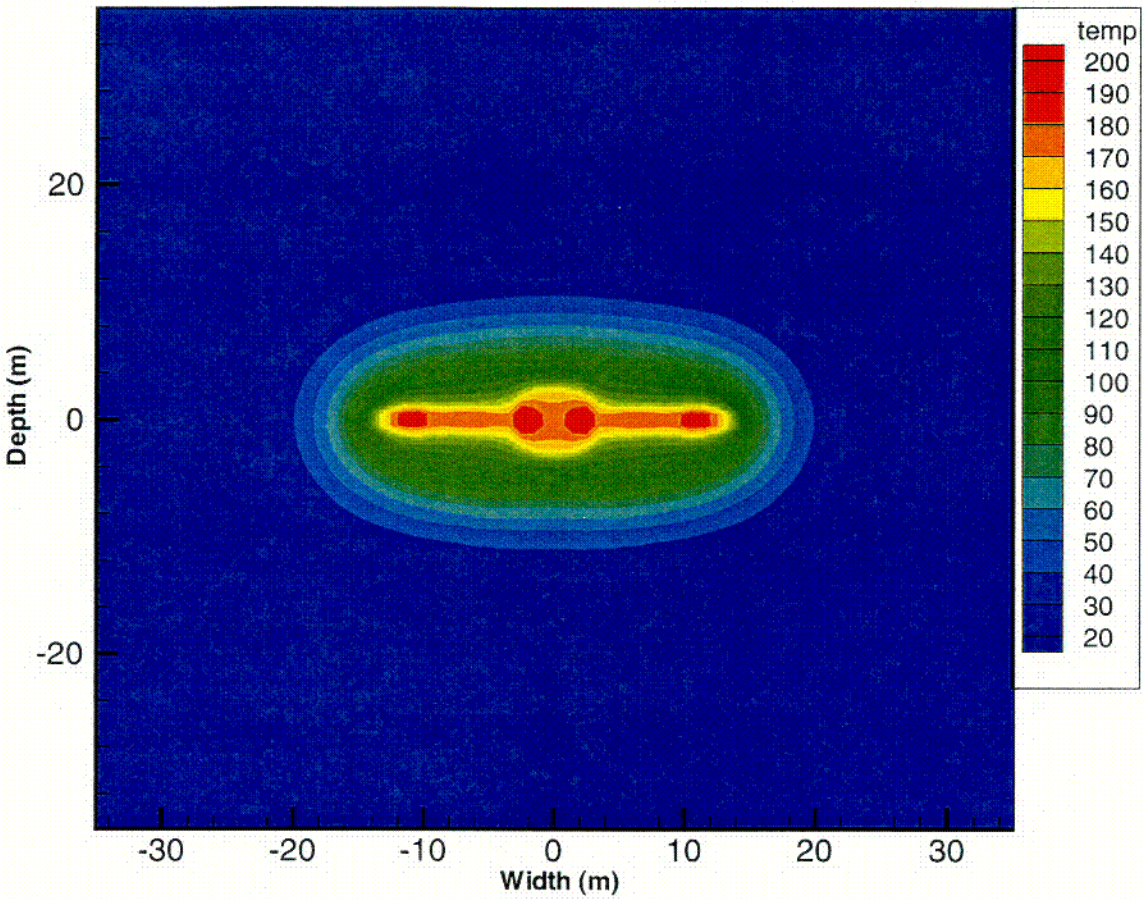


**Figure 4-13a. Contour plot of simulated matrix temperature for basecase property values except for a factor of 1,000 reduction in fracture permeability, a 20-percent reduction in thermal conductivity, and a mass loss of 80 mL/hr**



C12

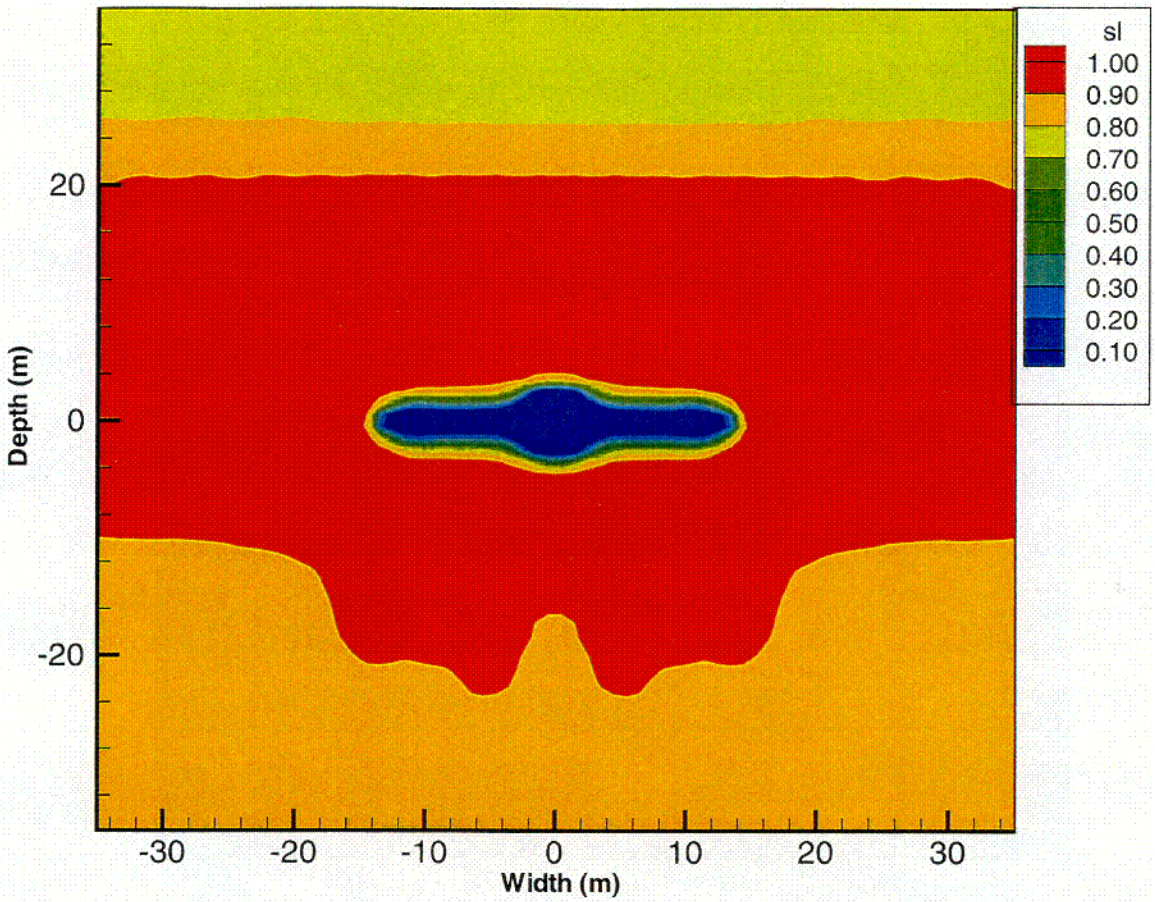


**Figure 4-13b. Contour plot of simulated matrix saturation for basecase property values except for a factor of 1,000 reduction in fracture permeability, a 20-percent reduction in thermal conductivity, and a mass loss of 80 mL/hr**



C13

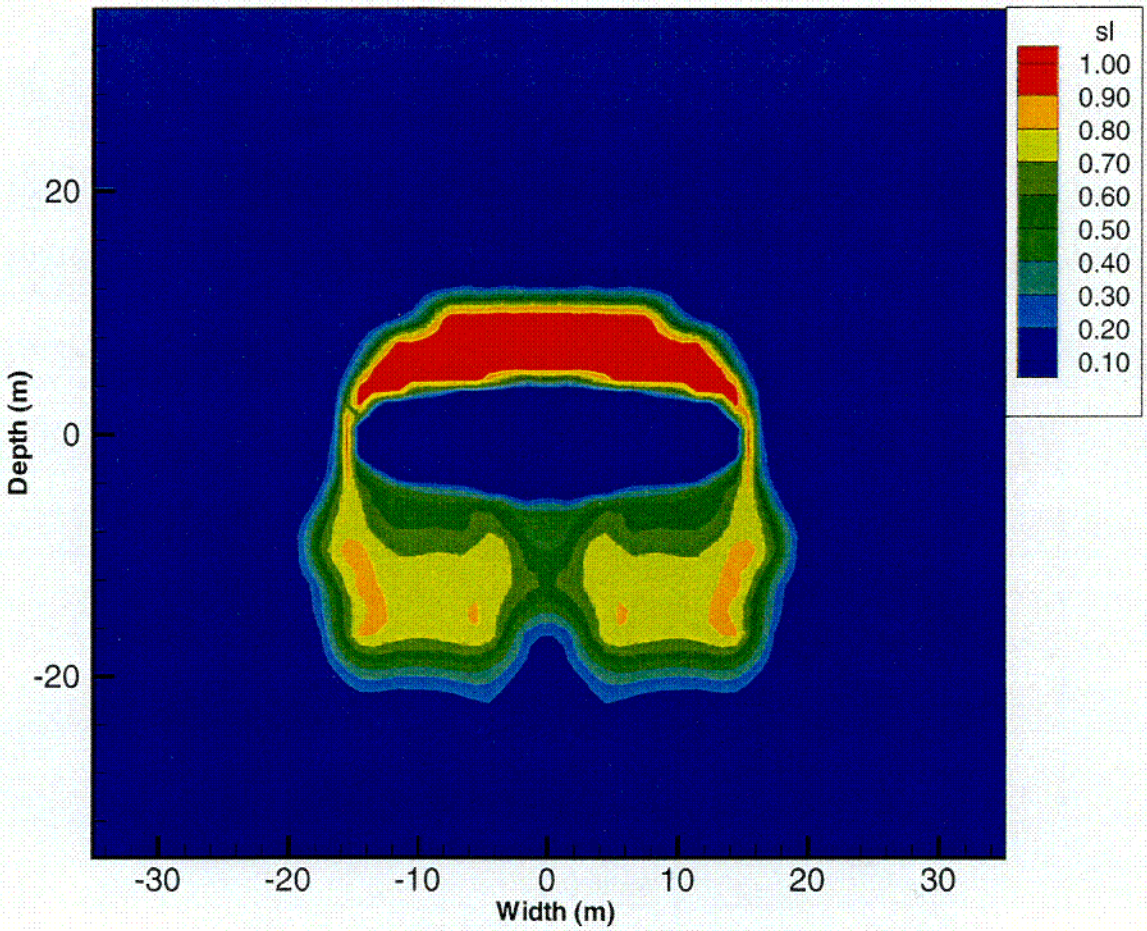


**Figure 4-13c. Contour plot of simulated fracture saturation for basecase property values except for a factor of 1,000 reduction in fracture permeability, a 20-percent reduction in thermal conductivity, and a mass loss of 80 mL/hr**



C14

# 5 DISCUSSION AND SUMMARY

This modeling study is an important part of assessing and developing confidence in the predictive models used to evaluate the safety case for the geologic repository at YM. This report was prepared as part of the DECOVALEX project to independently evaluate MULTIFLO, a TH model used by NRC in calculations to support their high-level waste regulatory program, and compare MULTIFLO results with results from other TH codes. The DST at YM has been used to provide a basis to assess the capability of the TH codes to simulate complex TH processes. This document contains recent results of this modeling effort.

Refinements in the numerical model used in previous modeling attempts reported in Green et al. (2000) reduced differences between predicted and simulated temperatures. Refinements that reduced the differences were a factor of 1,000 reduction in fracture permeability and a 20-percent reduction in thermal conductivity to all three geologic units simulated in the model. The large reduction in fracture permeability is believed to be realistic because of the large uncertainty both in fracture flow conceptual models and in the measurement of fracture properties, irrespective of the conceptual model selected. A 20-percent reduction in thermal conductivity is believed to be reasonable, as well, in part because measured property values may vary by similar amounts at field sites, and a 20-percent reduction in value may account for the bulk averaging of intact thermal conductivity measurements and voids due to lithophysae and fractures. Both assumptions will be evaluated in future investigations. In addition, the effect of mass loss through the thermal bulkhead was investigated. It was found that a mass removal of 80 mL/hr of liquid from the drift wall resulted in indistinguishable differences in predicted temperature, but small observable differences in predicted fracture saturation.

Additional potential refinements to the DST model identified during this study include the following:

- Convert the heater drift wall from a heat source and a mass sink to a heat source and Neumann or mixed boundary condition. This conversion would allow removal of water vapor in addition to liquid water from the heater drift-wall elements. Discrepancies in springline/drift-crown temperatures will be evaluated in this future exercise.

- Represent the gas relative permeability of the fractures using a Brooks-Corey (Brooks and Corey, 1966) formulation.

- Incorporate the active fracture model formulation (Lui et al., 1998).

- Evaluate calibrating the heat load imposed at the heater drift wall to incorporate heater drift canister heat losses experienced during the heating phase of the DST. Current simulations do not account for any heat losses to these heaters.

- Investigate the effect of differences in thermal loads between the inner and outer wing heaters.

# 6 REFERENCES


Birkholzer, J.T., and Y.W. Tsang. *Pretest Analysis of the Thermal-Hydrological Conditions of the ESF Drift-Scale Test.* Earth Sciences Division Level 4 Milestone Report SP9322M4. Berkeley, CA: Lawrence Berkeley National Laboratory. 1997.

Blair, S., T. Buscheck, L. DeLoach, W. Lin, and A. Ramirez. *Single Heater Test Final Report.* UCRL–ID–131491. Livermore, CA: Lawrence Livermore National Laboratory. 1998.

Bodvarsson, G.S., and T.M. Bandurraga. *The Site-Scale Unsaturated Zone Model of Yucca Mountain, Nevada, for the Viability Assessment.* LBNL–40376. Berkeley, CA: Lawrence Berkeley National Laboratory. 1997.

Brechtel, C.E., G. Lin, E. Martin, and D.S. Kessel. *Geochemical Characterization of the North Ramp of the Exploratory Studies Area.* SAND95–0488. Albuquerque, NM: Sandia National Laboratories. 1995.

Brooks, R.H., and A.T. Corey. Properties of porous media affecting fluid flow. *Journal of Irrigation and Drainage Engineering* 92: 61–88. 1966.

Green, R.T., D. Hughson, S. Painter, and M.E. Hill. *Evaluation of the Drift-Scale Heater Test Thermal-Hydrological Conceptual Model Data and U.S. Department of Energy Thermal Test Results—Status Report.* San Antonio, TX: Center for Nuclear Waste Regulatory Analyses. 2000.

Hirschfelder, J.O., C.F. Curtis, and R.B. Bird. *Molecular Theory of Gases and Liquids.* New York: John Wiley and Sons. 1954.

Klavetter, E.A., and R.R. Peters. *Estimation of Hydrologic Properties of an Unsaturated, Fractured Rock Mass.* SAND84–2642. Albuquerque, NM: Sandia National Laboratories. 1986.

Lichtner, P.C., M.S. Seth, and S. Painter. *MULTIFLO User's Manual MULTIFLO Version 1.2—Two-Phase Nonisothermal Coupled Thermal-Hydrologic-Chemical Flow Simulator.* Revision 2. Change 1. San Antonio, TX: Center for Nuclear Waste Regulatory Analyses. 2000.

Lui, H.H., C. Doughty, and G.S. Bodvarsson. An active fracture model for unsaturated flow and transport in fractured rock. *Water Resources Research* 34(10): 2,633–2,646. 1998.

Mualem, Y. A new model for predicting hydraulic conductivity of unsaturated porous media. *Water Resources Research* 12: 513–522. 1976.

Pruess, K. and T.N. Narasimhan. A practical method for modeling fluid and heat flow in fractured porous media. *Society of Petroleum Engineers Journal* 25(1): 14–26. 1985.

Somerton, W.H., A.H. El-Shaarani, and S.M. Mobarak. High temperature behavior of rocks associated with geothermal type reservoirs. *Society of Petroleum Engineers—44th Annual California Regional Meeting.* Paper SPE–4897. San Francisco, CA: Society of Petroleum Engineers. 1974.

TRW Environmental Safety Systems, Inc. *Ambient Characterization of the Drift-Scale Test Block.* BADD00000–01717–5705–00001. Revision 01. Las Vegas, NV: TRW Environmental Safety Systems, Inc. 1997a.

TRW Environmental Safety Systems, Inc. *Drift-Scale Test Design and Forecast Results.* B00000000–01717–4600–00007. Revision 00. Las Vegas, NV: TRW Environmental Safety Systems, Inc. 1997b.

TRW Environmental Safety Systems, Inc. *Total System Performance Assessment–Viability Assessment Analyses—Technical Basis Document.* B00000000–01717–4301–00001. Revision 01. Las Vegas, NV: TRW Environmental Safety Systems, Inc. 1998a.

TRW Environmental Safety Systems, Inc. *Thermal Test Progress Report #1.* Las Vegas, NV: TRW Environmental Safety Systems, Inc., 1998b.

TRW Environmental Safety Systems, Inc. *Thermal Test Progress Report #2.* Las Vegas, NV: TRW Environmental Safety Systems, Inc. 1998c.

TRW Environmental Safety Systems, Inc. *Drift-Scale Test As-Built Report.* BAB00000–01717–5700–0003. Revision 01. Las Vegas, NV: TRW Environmental Safety Systems, Inc. 1998d.

TRW Environmental Safety Systems, Inc. *Thermal Test Progress Report #3.* Las Vegas, NV: TRW Environmental Safety Systems, Inc. 1999a.

TRW Environmental Safety Systems, Inc. *Thermal Test Progress Report #4*, Las Vegas, NV: TRW Environmental Safety Systems, Inc. 1999b.

TRW Environmental Safety Systems, Inc. Thermal Tests Thermal-Hydrological Analyses/Model Report. Las Vegas, NV: TRW Environmental Safety Systems, Inc. 2000.

Tsang, Y.W., J. Apps, J.T. Birkholzer, B. Freifeld, M.Q. Hu, J. Peterson, E. Sonnenthal, and N. Spycher. *Yucca Mountain Single Heater Test Final Report.* LBNL–42537. Berkeley, CA: Lawrence Berkeley National Laboratory. 1999.

U.S. Nuclear Regulatory Commission. *Issue Resolution Status Report—Key Technical Issue: Evolution of the Near-Field Environment.* Revision 2. Washington, DC: U.S. Nuclear Regulatory Commission. 1999.

van der Kwaak, J.E., P.A. Forsyth, K.T.B. MacQuanie, and E.A. Sudicky. *WATSOLV, Sparse Matrix Iterative SolverPackage, User's Guide.* Waterloo, Ontario, Canada: Waterloo Centre for Groundwater Research, University of Waterloo. 1995.

van Genuchten, M. Th. A closed-form equation for predicting the hydraulic conductivity of unsaturated soils. *Soil Science Society of American Journal* 44: 892–898. 1980.

Walton, J., and P. Lichtner. *Quasi-Steady State Model for Coupled Liquid, Vapor, and Heat Transport: Application to the Proposed Yucca Mountain High-Level Waste Repository.* San Antonio, TX: Center for Nuclear Waste Regulatory Analyses. 1995.